

CLIMATE FORCINGS AND THE INITIATION OF LOW-LATITUDE ICE SHEETS
DURING THE NEOPROTEROZOIC VARANGER GLACIAL INTERVAL

Mark A. Chandler

NASA/Goddard Institute for Space Studies and the
Center for Climate Systems Research at Columbia University
2880 Broadway, New York, New York 10025
mchandler@giss.nasa.gov

and

Linda E. Sohl

Department of Earth and Environmental Sciences and the
Lamont-Doherty Earth Observatory of Columbia University
Palisades, New York 10964
sohl@ldeo.columbia.edu

Submitted to

Journal of Geophysical Research – Atmospheres

Revised-January 2000

Abstract. The GISS GCM was used to determine if a diverse set of climate forcings, alone or in combination, could have initiated the low-latitude ice sheets of the Varanger (~600 Ma) glacial interval. The simulations use a realistic reconstruction of the paleocontinental distribution and test the following forcings, alone and in combination: 6 percent solar luminosity decrease, four atmospheric CO₂ scenarios (1260 ppm, 315 ppm, 140 ppm and 40 ppm), a 50% increase and 50% decrease in ocean heat transports, and a change in obliquity to 60°. None of the forcings, individually, produced year-round snow accumulation on low-latitude continents, although the solar insolation decrease and 40 ppm CO₂ scenarios allowed snow and ice to accumulate at high and mid-latitudes. Combining forcings further cools the climate: when solar luminosity, CO₂ and ocean heat transports were all decreased, annual mean freezing and snow accumulation extended across tropical continents. No simulation would have initiated low-latitude glaciation without contemporaneous glaciation at higher latitudes, a finding that matches the distribution of glacial deposits, but which argues against high obliquity as a cause of the Varanger ice age. Low-level clouds increased in most scenarios, as did surface albedo, while atmospheric water vapor amounts declined; all are positive feedbacks that drive temperatures lower. In the most severe scenario, global snow and ice cover increased to 68%, compared to 12% under modern conditions, and water vapor dropped by 90%. These results do not necessarily preclude a "snowball" Earth climate scenario for the Varanger glacial interval. However, either more severe forcings existed, or radical changes occurred in the ocean/atmosphere system that are unaccounted for by the GCM. Also, as sea ice extent increased in these experiments, snow accumulation began to decline, owing to an increasingly dry atmosphere. Under snowball Earth conditions glaciation would be impossible, since the hydrological cycle would all but cease if the atmosphere's primary moisture source were cut off.

1. INTRODUCTION

The Neoproterozoic Era stands out from any other time interval before or since in terms of the profound changes in how various Earth system processes functioned [see e.g., *Chumakov and Elston*, 1989; *Knoll and Walter*, 1992]. Earth's climatic system was no exception; it too experienced significant shifts to alternate modes of operation in the ocean, atmosphere and biosphere in association with a variety of key tectonic and environmental events (see Figure 1). For more than 1 billion years after the Huronian glaciation (~2.2 Ga), Earth's climate had been locked into a warm, equable mode, as evidenced by the dearth of glacial deposits in the geologic record [e.g., *Hambrey*, 1994]. During the Neoproterozoic, however, the world cooled dramatically as it entered the first of two broad intervals of widespread glaciation: the Sturtian glaciation (~750-720 Ma), and the Varanger glaciation (~610-575 Ma) [see *Knoll and Walter*, 1992; *Bowring and Erwin*, 1998]. Uncertainties in age dating of, and lithostratigraphic relationships between, glacial deposits of each interval leave open the possibility that glaciation in various regions was diachronous [see, e.g., *Kröner*, 1977], perhaps alternating with interglacial intervals that may have been at least as warm as the present interglacial. What is especially remarkable about the Neoproterozoic glaciations is their severity; recent paleomagnetic evidence demonstrates that during both major glaciations at least some land regions, which were located equatorward of 20° latitude, were affected by continental-scale glaciation at elevations down to sea level [e.g., *Schmidt and Williams*, 1995; *Park*, 1997; *Sohl et al.*, 1999].

Various explanations and models have been proposed over the past forty years in an effort to account for the phenomenon of Neoproterozoic low-latitude glaciation [*Williams*, 1975, 1993; *Crowell*, 1983; *Sheldon*, 1984; *Marshall et al.*, 1988; *Kirschvink*, 1992; *Crowley and Baum*, 1993]. Explanations built upon geological evidence (i.e., paleomagnetism, lithostratigraphy) are chiefly models for ice distribution that often do not consider what climatic processes may have feasibly produced such a distribution [e.g., *Kirschvink*, 1992; *Williams*, 1993]. Climate modeling experiments have so far used simplified scenarios, such as assigning modern or idealized continental distributions and surface conditions, which bear little resemblance to any geography

that actually existed, or by using highly parameterized representations of the physical processes. In order to solve the Neoproterozoic puzzle, we believe it is necessary to incorporate realistic constraints based upon geological and geophysical data and to continue to improve upon our ability to simulate the critical climatic processes. In this paper, we explore the first of a series of climatic experiments, aimed in this case at identifying which combination of basic climate forcings may have played a role in permitting low-latitude glaciation to occur during the Varanger glacial interval in the late Neoproterozoic.

2. BACKGROUND

2.1. *The Debate*

The first researchers to suggest the existence of low-latitude glaciation during the Neoproterozoic [Harland and Bidgood, 1959; Girdler, 1964; Harland, 1964] were struck by the apparent close spatial and temporal relationships between the Sturtian and Varanger glacial deposits and carbonates that were presumably deposited in warm, tropical settings as they commonly are today [e.g., Spencer, 1971; Chumakov and Elston, 1989; cf. Walter and Bauld, 1983; Fairchild *et al.*, 1989]. It was suggested that the world had essentially frozen over [Harland, 1964], a condition that later came to be called the "snowball Earth" [Kirschvink, 1992; Hoffman *et al.*, 1998]. The results of early paleomagnetic studies supporting the low-latitude glaciation hypothesis [e.g., Harland and Bidgood, 1959; Girdler, 1964], and additional studies conducted in the 1980's and early 1990's [e.g., Morris, 1977; McWilliams and McElhinny, 1980; Kröner *et al.*, 1980; McWilliams and Kröner, 1981; Zhang and Zhang, 1985; Embleton and Williams, 1986; Li Yianping *et al.*, 1991] were later called into question by Meert and Van der Voo [1994]. They pointed out various problems (i.e., poor lithostratigraphic correlations between rocks actually sampled and the glacial rocks, possible remagnetizations, and improved data reflecting at least mid-latitude depositional settings) that weakened the low-latitude interpretation of the glacial rocks. However, paleomagnetic data from the South Australian Varanger-age glacial rocks themselves [Embleton and Williams, 1986; Schmidt *et al.*, 1991] withstood Meert and Van der Voo's scrutiny, and additional studies have since confirmed the rocks' low depositional paleolatitude [Schmidt and

Williams, 1995; Sohl et al., 1999]. New and improved paleomagnetic data from the Sturtian-age glacial deposits of northwestern Canada now suggest that these rocks, too, were deposited below 20° latitude [*Park, 1997*]. More paleomagnetic data are needed to ascertain the full distribution of glacial deposits for both Neoproterozoic glacial intervals, but the data already in hand reveal a climatic system capable of extremes that most paleoclimate researchers seldom consider.

Questions surrounding the sedimentological evidence for the glacial origins of the Sturtian and Varanger-age deposits have cited concerns that the deposits are actually misidentified debris flows, or even meteorite impact ejecta blankets [*Oberbeck et al, 1993; Rampino, 1994*]. The sedimentological evidence in support of the glacial interpretation is, however, quite strong. There are thick successions (thousands of meters) of *marine* diamictites containing glacially striated and faceted stones, and laminated siltstones containing dropstones that are inferred to have been ice-rafted rather than transported by some other means [e.g., *Vorren et al., 1983; Thomas and Connell, 1985; Bennett et al., 1994*]. Rare, glacially striated pavements, in some cases associated with valleys hundreds of meters deep, reveal the erosive activity of ice sheets [*Biju-Duval and Gariel, 1969; Christie-Blick, 1983; Edwards, 1984; Karfunkel and Hoppe, 1988*]. Periglacial features, such as fossil sand wedges and frost-heaved blocks, are also found in connection with a number of the glacial deposits [e.g., *Nystuen, 1976; Deynoux, 1982; Williams and Tonkin, 1985; Deynoux et al., 1989; Zhang, 1994*]; such features require consistently cold temperatures, and cannot be confused with non-glacial phenomena.

2.2. Previous Modeling Studies

A number of climate forcing factors have been called upon to explain the unusual climatic patterns of the Neoproterozoic. These include: continentality (paleogeographic distribution of land), atmospheric greenhouse gas levels, reduced solar luminosity, the obliquity of the planet, the Earth's rotation rate, and altered ocean heat transports [e.g. *Williams, 1975, 1993; Crowley and Baum, 1993; Oglesby and Ogg, 1998; Jenkins and Frakes, 1998; Jenkins and Smith, 1999*]. In this study, we have modified five of those six forcings (excluding rotation rate) to explore their effects on air temperatures, as well as snow and ice cover. A number of these forcings are coupled

to each other via feedback mechanisms and are likely to have acted in concert during the Neoproterozoic. Thus, in addition to analyzing their individual effects, our study examines the combined effects of carbon dioxide change, solar luminosity decrease and altered ocean heat transports to determine what forcings may have been required to cause the growth and persistence of large-scale ice sheets at low ($< 20^\circ$) latitudes.

Crowley and Baum [1993] used a two-dimensional energy balance model to shed light on the types of climate forcing extrema that may have been required to generate the cold low-latitude temperatures of the Varanger ice age. They recognized that the lower solar luminosity of that time certainly could have played an important role in the Neoproterozoic glaciations. (In fact, many studies have focused on why the early Earth's climate was not *always* cold given the lower levels of solar forcing). Crowley and Baum's experiments concentrated on solar effects as well as altered CO₂ levels and obliquity in sensitivity experiments, but did not discuss those simulations in detail. More recently, *Jenkins and Frakes* [1998] and *Jenkins and Smith* [1999] used the GENESIS GCM (v1.02) to explore the role of increased rotation rate, reduced solar forcing, reduced CO₂, and orography on the climate of an idealized tropical supercontinent. Their results differed greatly depending upon the method used to simulate the sea surface temperature (SST) response; specified SST simulations showed little snow accumulation on the tropical continent, yet snow accumulation was substantial when they employed a mixed-layer ocean model. Jenkins and Smith [1999] found that their model could produce an ice-covered ocean if they lowered solar luminosity, dropped atmospheric CO₂ to 100 ppm, and increased the rotation rate to 18 hrs/day (the rate for the Varanger interval is about 21.9 hrs/day). Using modern levels of CO₂ (340 ppm in their study) or greater they found that low-latitude ocean waters remained open. In another study, *Oglesby and Ogg* [1998] used the NCAR CCM1, and modern geography, to simulate the effects of obliquity changes on climate, while also varying CO₂ levels and solar luminosity. At high obliquity (70°) and reduced solar radiation, they found that sea ice formed, and snow accumulated, year-round in the tropics. Our simulations seek to take the exploration of the Neoproterozoic climate a step further

through the use of a broader range of forcing factors and, most importantly, to incorporate the use of a more realistic paleogeographic reconstruction of the Varanger continental distribution.

3. CLIMATE MODEL AND FORCINGS

3.1 *The GISS GCM*

We use the Goddard Institute for Space Studies general circulation model, version II (GISS GCM), a detailed description of which is given by *Hansen et al.* [1983]. The GISS GCM is a three-dimensional model which solves numerically the physical conservation equations for energy, mass, momentum and moisture as well as the equation of state. The version we used has a horizontal resolution of 8° latitude by 10° longitude, nine layers in the atmosphere extending to 10mb, and two ground hydrology layers. The model accounts for both the seasonal and diurnal solar cycles in its temperature calculations. Cloud particles, aerosols, and radiatively important trace gases (e.g. carbon dioxide, methane, nitrous oxides) are explicitly incorporated into the radiation scheme. Large-scale and convective cloud cover are predicted, and precipitation is generated whenever supersaturated conditions occur. Snow depth is based on a balance between snowfall, melting and sublimation.

Sea surface temperatures (SST) are calculated using model-derived surface energy fluxes and specified ocean heat convergences. The ocean heat convergences vary both seasonally and regionally, but are otherwise fixed. This is the primary mixed-layer ocean model developed for use with the GISS GCM, full details of which are described in *Russell et al.* [1985], and in appendix A of *Hansen et al.* [1988]. In brief, the convergence (divergence) at each grid cell is calculated based on the heat storage capacity of the surface ocean and the vertical energy fluxes at the air/sea interface. The annual maximum mixed-layer depth, which varies by region and season, has a global, area-weighted value of 127 meters. Vertical fluxes are derived from specified SST control runs: observed SSTs are used for the modern and, for the Varanger, an SST distribution that preserves the zonally-averaged meridional SST gradient is employed. The only modification we have introduced to the original method of *Russell et al.* [1985] is to use five harmonics, instead of two, in defining the seasonally-varying energy flux and upper ocean energy storage. This

improves the accuracy of the approximations in regions of seasonal sea ice formation. The technique reproduces modern ocean heat transports that are similar to those obtained by observational methods [Miller *et al.* 1983]. By deriving vertical fluxes and upper ocean heat storage from a run with appropriate paleogeography, it provides a more self-consistent method for obtaining ocean heat transports from paleoclimate scenarios that use altered ocean basin configurations.

The role of the ice/albedo feedback is certain to be important in experiments that produce significant changes in sea ice and snow cover. Hansen *et al.* [1983] describe fully the snow and ice parameterizations used in the GISS GCM. The albedo of snow is a function of both depth and age. Fresh snow has an albedo of 0.85 and ages within 50 days to a lower limit of 0.5. The sea ice parameterization is thermodynamic with no relation to wind stress or ocean currents. Below -1.6°C ice of 0.5 m thickness forms over a fractional area of the grid box and henceforth grows horizontally as needed to maintain energy balance. Surface fluxes change the ocean water and sea ice temperature in proportion to the area of a grid cell they cover. Conductive cooling occurs at the ocean/ice interface, thickening the ice if the water temperature remains at -1.6° . Sea ice melts when the ocean warms to 0°C and the SST in a grid box remains at 0°C until all ice has melted in that cell. The albedo of sea ice (snow-free) is independent of thickness and is assigned a value of 0.55 in the visible and 0.3 in the near infrared, for a spectrally weighted value of 0.45.

We assign a uniform height of 50 meters to all land areas as the topographic relief for this time period is not well known. Experiments using an idealized continent and mountain range have shown that the role of orographic belts may be an important factor influencing the initiation of low-latitude glaciation. Experiments using interpretations of continental relief, based perhaps on tectonic constraints or sedimentary analysis, will at some point provide information on the simulated climate's sensitivity to this simplification, but we do not pursue that issue in this study. The GCM requires the assignment of vegetation categories to each grid cell containing land, and the assignments are integral to the ground hydrology parameterization of our GCM [Hansen *et al.*,

1983; Matthews, 1985]. Since vascular land plants had not yet evolved 600 million years ago, we mimic the lack of land vegetation by assigning desert conditions at all land locations.

It is common practice, when comparing a large number of simulations in which forcings are altered, to integrate each simulation over a few decades until it reaches radiative equilibrium. All of our experiments were run for 60 simulated years; we present results that were averaged over the final five years of those simulations.

3.2. Altered Forcings and Boundary Conditions

A complete list of the climate forcings and geographic boundary conditions applied to each of the simulations in this study is given in Table 1. A detailed description of the forcings and reconstructed Varanger geography follows:

3.2.1. Paleogeographic Distribution. One of the hypotheses proposed to explain the existence of low-latitude glacial deposits has suggested that glaciation could have occurred while the continents were fully emergent in a ringworld configuration centered on the equator [Piper, 1982; Marshall *et al.*, 1988; Worsley and Kidder, 1991], or at least located chiefly in low to intermediate latitudes [Kirschvink, 1992; Hoffman *et al.*, 1998]. In this scenario, ice sheets would have nowhere to develop *but* at low-latitudes, and thus the phenomenon of low-latitude glaciation could be partly explained as the consequence of a unique geographic configuration. As noted above, however, more recent paleomagnetic data [e.g., Torsvik *et al.*, 1992, 1996] do not support a ringworld reconstruction for the late Neoproterozoic; combining these data with paleocontinental reconstructions that have subsequently emerged [e.g., Powell *et al.*, 1993; Dalziel, 1997], it now seems likely that most land mass was concentrated in the southern hemisphere during the Varanger glaciation.

Previous modeling studies [Crowley and Baum, 1993; Jenkins and Smith, 1999] have used sensitivity tests to examine the effect of continental distribution on the Neoproterozoic climate. Our objective is to explore the influence of other climate forcings in the presence of a realistic paleocontinental distribution. Consequently, as part of this study, we developed a paleocontinental reconstruction for the Varanger glacial interval (~600 Ma, see Figure 2), for use

as a GCM boundary condition in our simulations. This reconstruction is necessarily tentative, as reliable paleomagnetic data are not abundant and age constraints on lithostratigraphic relationships are not well defined. Nevertheless, it is possible to place bounds on paleogeography that are reasonable for the purposes of this study. The principal guides for the overall paleogeographic distribution at ~600 Ma are the reconstruction of the early to mid-Neoproterozoic supercontinent Rodinia [Moore, 1991; Dalziel, 1991] and the latest Neoproterozoic-Early Cambrian reconstruction of Gondwanaland [e.g., Hoffman, 1991; Dalziel, 1997]. Paleomagnetic data provide the framework for our Varanger reconstruction; these data place Australia at low paleolatitudes [Schmidt and Williams, 1995; Sohl *et al.*, 1999], Baltica (Scandinavia) at high to intermediate paleolatitudes [Torsvik *et al.*, 1992, 1996; Elming *et al.*, 1993], and Laurentia (North America) at intermediate to high paleolatitudes [Park, 1994]. Laurentia and Australia are separated by >3000 km, as reflected by a divergence in their respective apparent polar wander (APW) paths and the lithostratigraphic record at ~700 Ma [Powell *et al.*, 1993, 1994; cf. Veevers *et al.*, 1997]. Strong lithostratigraphic relationships tie other land masses to those whose paleolatitude is constrained by paleomagnetic data. Antarctica and India are bound to Australia as components of East Gondwana [e.g., Meert and Van der Voo, 1997], which extends across the equator to intermediate latitudes; this long-lived triumvirate endures until the Cenozoic. Siberia is joined to Laurentia's northwestern boundary through the Early Cambrian [Pelechaty, 1996], and Baltica is joined to Laurentia's northeastern boundary until the latest Neoproterozoic-Early Paleozoic [Torsvik *et al.*, 1992, 1996].

The positions of other large land masses are less certain. The latitudinal position of South China is unconstrained, but its position in our model between East Gondwana and western Laurentia is in agreement with the hypothesis of Li *et al.* [1995]. West Gondwana (Amazonia and La Plata, plus West Africa and the Congo Craton) is placed at intermediate to high paleolatitudes based upon the plate motions required for the mid-Cambrian consolidation of Gondwanaland after the breakout of Laurentia [Hoffman, 1991; Powell *et al.*, 1993; Meert and Van der Voo, 1997]. The Kalahari Craton is located at the end of Antarctica opposite Australia as part of the Rodinian

reconstruction, where it is assumed to remain through the consolidation of Gondwanaland [Hoffman, 1991; Dalziel, 1997]. The location of Armorica (parts of central Europe) with respect to West Gondwana is inferred from the similarity of the Armorican and West Gondwanan APW paths for the late Neoproterozoic and early Cambrian; such similarity suggests that these masses were connected at that time [Hagstrum *et al.*, 1980; Van der Voo *et al.*, 1980]. The low-latitude locations of the remaining land masses included in this reconstruction – North China, Tibet, Kazakhastania and Mongolia – are largely arbitrary. Hoffman [1991] suggested that Kazakhastania and Mongolia may have been in close proximity to Siberia as part of the Rodinian supercontinent, but there is no evidence at present to suggest that a close relationship existed at ~600 Ma.

In order to transfer our paleogeographic reconstruction to the coarse resolution grid (8° x 10°) used for this study, we needed to estimate the total land area available for glaciation, including exposed continental shelves. We approximated that area by rounding off the modern values for individual geographic regions included in the reconstruction and adding 10% as an estimate of shelf area available. Such estimates are a bit conservative, and as a result the total land area in our reconstruction (~1 x 10⁸ km²) is only about 60% of the modern value. However, since our reconstruction includes the largest coherent continental masses known to exist at that time, it is probable that any additional land area was scattered in masses too small to affect the development and distribution of large-scale ice sheets.

3.2.2. Atmospheric CO₂. For many periods during Earth history prior to the Quaternary, it is believed that the levels of atmospheric greenhouse gases, particularly CO₂, were higher than at present in order to compensate for a less luminous sun [Berner, 1991, 1994; Kasting, 1988, 1991, 1992, 1997; Crowley and Baum, 1993]. In the earliest periods of Earth history, heating of the Earth's surface owing to increased CO₂ may have helped offset the reduction in solar radiation. In fact, evidence for the presence of liquid water as early as the Archean seems to require greenhouse warming of the planet for much of early Earth history. To approximate a warm, equable climate under lower luminosity conditions, such as those that might have existed in the early Neoproterozoic (~1,000 Ma), we ran experiments using 4 times modern (ca. 1958) CO₂ levels

(1260 ppm). This is somewhat higher than the 840 ppm estimate of *Carver and Vardavas* [1994] for 600 Ma. However, it lies within the error estimates of *Berner* [1991, 1994] and is useful for comparison with other warm climate GCM sensitivity experiments. We do not suppose that an enhanced greenhouse effect is a likely mechanism for cooling the planet, but we surmise that glacial initiation, were it triggered solely by non-atmospheric forcings, would have needed to overcome the radiative effects of increased atmospheric CO₂ levels. It is also possible that a warmer atmosphere, holding more moisture, may have increased high latitude glaciation by providing increased snowfall rates.

Of course, the evidence for extreme Neoproterozoic ice ages may suggest that these particular periods were times of CO₂ drawdown instead. Therefore, we ran simulations with atmospheric CO₂ levels set to 315 ppm, 140 ppm, and 40 ppm, as well. The value of 315 ppm is the approximate amount of CO₂ in the atmosphere in 1958 (the first year for which direct measurements are available) and is the amount used in the GISS current climate control simulations; 140 ppm is one-half of the accepted preindustrial value; and 40 ppm was chosen as an extreme example, which deliberately corresponds to the extreme experiments run by *Crowley and Baum* (1993). To further put these CO₂ forcings into context, our reduced CO₂ experiments use values that are from 50 ppm to 150 ppm lower than minimum levels found at the last Pleistocene glacial maximum [see, e.g., *Schneider*, 1987].

An "effective" level of atmospheric CO₂ is sometimes used to simulate the combined effect of changes in other greenhouse gases within climate models [e.g. *Washington*, 1992]. The GISS GCM, however, explicitly calculates the radiative effects of all significant greenhouse gases. We acknowledge that other greenhouse gases, particularly methane, may have played a role in Neoproterozoic climate changes, and to some extent the radiative effects are likely to have been similar to those produced by CO₂ changes. However, in the case of extreme changes, the radiative impact and feedbacks associated with methane may be unique from those of CO₂; thus our simulations may not be appropriate for drawing general conclusions about the effect of all greenhouse gas changes.

3.2.3. Solar Luminosity. Models of stellar evolution have suggested that a G-type yellow star, such as the Sun, should have been as much as 30% less luminous during the earliest history of the Earth [Sagan and Mullen, 1972; Gough, 1981]. By the Varanger, ~600 Ma, the sun would have increased its energy output, but would still have been between 4% and 6% less luminous than today [e.g., Gough, 1981]. In addition to our simulations which use modern solar luminosity, we chose to run simulations with solar input decreased to 94% of the present-day value (solar flux was reduced from the modern value of 1367 Wm^{-2} to 1285 Wm^{-2}). Solar radiation is reduced in the model by decreasing the total amount of shortwave radiation entering the top of the atmosphere, and is proportionally reduced at all wavelengths.

The paradox of a theoretically faint young sun existing simultaneously with liquid water, for which there is significant evidence, has long concerned researchers exploring the climate of the early Earth, though the paradox is more clear for Archean times (where luminosity was greatly reduced) than for the Neoproterozoic. As noted above, many believe that increased levels of greenhouse gases (carbon dioxide, or perhaps methane) may have been present in the atmosphere and, therefore, would have absorbed enough longwave energy to offset some or all of the reduced amount of incoming solar radiation [Sagan and Mullen, 1972; Newman and Rood, 1977; Owen *et al.*, 1979; Kasting, 1992]. In addition, it has been speculated that cloud feedbacks may have helped to stabilize temperatures early in Earth's history [Rossow, 1982]. The GISS GCM predicts cloud cover interactively, thus their feedback potential is a diagnostic result for all experiments.

3.2.4. Ocean Heat Transports. The transport of heat by ocean circulation is critical to the distribution of temperatures on the planet [Peixoto and Oort, 1992]. Today the oceans transport heat, on an annually averaged global basis, away from the tropics and subtropics and into the middle and high latitudes. This transport is generated by both the wind-driven ocean circulation (for example, the Gulf Stream and Kuroshio currents) and by the large-scale thermohaline circulation, primarily by the production of deep water in the North Atlantic ocean. A number of climate studies and climate modeling experiments [Baker, 1977; Broecker and Denton, 1989; Covey and Barron, 1988; Rind and Chandler, 1991; Trenberth and Solomon, 1994] attest to the

climate effects that can be generated by changes in ocean heat transports. Such changes affect more than temperature gradients because they modify a variety of important climate feedback mechanisms, which ultimately control many aspects of global climate. Paleoclimate simulations, both colder and warmer than the present, implicate changes in ocean circulation and ocean heat transport as an important factor in past climate change [Barron *et al.*, 1993; Chandler *et al.*, 1992; O'Connell *et al.*, 1996; Webb *et al.*, 1997]. We have simulated the potential effects of both increased and decreased poleward ocean heat transports on the Varanger climate. Our standard-ocean Neoproterozoic simulations use ocean heat fluxes that yield zonally-averaged, meridional transports that are comparable to modern values. The transports are necessarily modified since the Neoproterozoic ocean basin configurations are much different than modern. The decreased and increased ocean heat transport scenarios use ocean transports that are one-half ($OHT_{0.5}$) and 1.5 times ($OHT_{1.5}$) the modern global value. The zonal mean of the annual ocean heat transports for modern and Varanger simulations are shown in figure 3.

3.2.5. Obliquity. Williams [1975, 1993, 1994a] has suggested that low latitudes would be preferentially glaciated if Earth's obliquity were 54° or more. A high obliquity would also be capable of producing the frigid climate and strong seasonality necessary to create permafrost and related features observed in some Varanger-age Australian glacial sediments [Williams and Tonkin, 1985]. Williams theorizes that a high obliquity could have resulted from a large impact early in Earth's history, such as the impact believed to have produced the Moon [e.g., Hartmann and Vail, 1986]. Reduction of Earth's obliquity to present-day values could then have been accomplished through an obliquity-oblateness feedback produced by ice sheet loading and unloading near the equator, in combination with dissipative processes at the core-mantle boundary during a major resonance of the fluid core [Williams, 1993, 1994b]. In most of our simulations we use the present-day obliquity value of 23.5° , but we ran one simulation in which the only altered conditions were the Varanger paleogeography and the obliquity, which was changed to 60° .

4. CLIMATE SIMULATION RESULTS

The plausibility of forming continental ice sheets at low latitudes depends largely on the temperature and moisture regime over low-latitude land areas; generally, the climate must be conducive to annual snow accumulations that withstand summertime melting. Glacial initiation requires that at least some continental regions exist where snow accumulation exceeds ablation. The climate variables of greatest direct significance, therefore, are the surface air temperature and snow accumulation.

Figure 4 shows the annual average, global surface air temperature as it approaches equilibrium in each of the simulations. All experiments, except the obliquity simulation, are at or near radiative equilibrium within the 60-year period of the experiments. Maps, for all simulations of annual mean surface air temperature are presented in figure 5 and figure 6 shows the same for the snow and ice accumulation results. Table 2 gives a summary of temperature and snow accumulation results for the various simulations. It also shows results for a number of the feedback quantities that result from, and help drive, the climate change including: cloud cover, albedo, and atmospheric water vapor. The color maps (Figures 5 and 6) and Table 2 begin with the Modern (M) and Varanger (V) control simulation results, in which all forcings are set at current climate levels. The altered forcing simulation results (in Table 2 and Figures 5 and 6) are arranged, and numbered, in order of decreasing tropical temperature.

4.1 Surface Air Temperature Response to Individual Forcings.

Globally averaged, annual surface air temperatures in the Varanger simulations encompass a broad spectrum of results that range from much warmer to much colder than modern. Surface air temperatures in the simulations are greater than 28°C with quadrupled CO₂ levels and are less than -20°C when the most extreme forcings are combined. For comparison, the GISS GCM modern climate control run has an annual average surface air temperature of 13.4°C. Annual average tropical temperatures are about 25.1°C in our modern simulation, whereas the tropical temperatures in the Varanger simulations vary from a high of 36.6°C under increased CO₂ conditions to a low

below freezing (-1.1°C) when extreme forcings are used. Given the variety of forcings applied in these experiments, a wide range of results could be expected. However, the relative significance of global average climate to that of the tropics is not entirely straightforward. Global average temperature is often not the best indicator of the forcings' relative effects on tropical temperatures, particularly when forcings that alter the relative amounts of low versus high latitude radiation are used.. For example, had we ordered the simulations in table 2 by decreasing global temperature, instead of by tropical temperature, the relative positions of the obliquity and ocean heat transport experiments would change significantly.

In spite of the large continent/ocean realignment, the reconstructed paleogeography does not have a dramatic influence on the global air temperature or the potential for ice sheet initiation in the model. A slight increase of surface air temperature occurs when the Varanger paleogeography is used in place of the modern geographic configuration (Table 2). Global average temperature increases about 1°C while tropical temperatures warm by a modest 0.3°C . The modest global warming is the result of increased snow cover, a slight decrease in low-level clouds, and a small increase in high clouds (Table 2). Together these changes lead to lower ground and planetary albedo values. There is also a modest increase in atmospheric water vapor, which is probably attributable to the greater areal coverage of ocean versus land in the Northern Hemisphere and in the tropics during the Varanger (difference in continental distribution shown in Figure 5, Maps M and V). Surface air temperatures over the southern continent were 5° to 15°C warmer with the Varanger paleogeographic reconstruction, a result of the lower elevations and lower albedos on the Varanger southern high-latitude continent. It is important to note here that our Varanger paleogeographic reconstruction does not include the initial existence of continental ice sheets (though sea ice with an approximately modern seasonal distribution was included for the initiation of each simulation). The modern global climate is cooled slightly by the Greenland and Antarctic ice sheets and this alone may account for much of the minor warming found when we switch to the Varanger paleogeography.

Despite the increased hemispheric asymmetry in continental distribution, the absence of a large polar ice sheet results in a more symmetrical surface temperature distribution in the Varanger. In subsequent experiments, in which snow on the continents expands, the continued lack of significant asymmetry in the cooler climates may seem somewhat surprising. However, in the cooler climates, sea ice forms a platform over the northern hemisphere ocean, minimizing “continentality” differences between the two hemispheres (Figure 6).

As might be expected, the simulations with 1260 ppm atmospheric CO₂ levels led to the warmest climates, raising global temperature by nearly 14°C and yielding tropical temperatures that exceeded 36°C (Table 2 and Figure 5, Map 1). Global atmospheric water vapor more than doubles, ground albedo falls by 30%, and low cloud amounts decline, all of which constitute positive feedbacks to warming. High clouds also decrease as upper level atmospheric temperatures warm and less condensation occurs at high altitudes, an effect that constitutes a small negative feedback to further warming. The Varanger simulations using one-half the pre-industrial atmospheric CO₂ level (140 ppm) resulted in a 7.4°C global cooling (Figure 5, Map 5), which is colder than the global temperature associated with previous GISS GCM simulations of the Pleistocene last glacial maximum [*Rind*, 1986, 1988]. While not wanting to stretch the Pleistocene analogy too far, this at least suggests that mid-latitude ice sheet formation could have commenced under such conditions during the Varanger. Low latitudes cool by about 5°C, but this still leaves the annual average temperatures in the tropics at around 20°C, strongly indicating that this type of “intermediate” reduction in CO₂ by itself is an unlikely candidate to produce significant low-latitude continental glaciation. Reducing CO₂ further to 40 ppm, resulted in an additional 10° to 11°C of cooling both globally and in the tropics. Global annual average temperatures drop below freezing (-4.3°C), yet tropical temperatures never get much colder, in the zonal average, than about 8°C (Table 2). The lowest latitude to which zonally averaged freezing temperatures extend is about 36°, however, the freezing line does extend further towards the equator in certain regions. Over the ocean, east of East Antarctica, and across several mid- to low-latitude continents such as Siberia, South China,

and East Antarctica (refer to Figure 2) annual average freezing extends to about 25°S (see Map 8 in both figures 5 and 6).

The 6% solar luminosity decrease yields global mean temperatures which are also below freezing, with an annual average of -4.0°C . Tropical temperatures decrease to 9.4°C , which is considerably cooler than the 140 ppm CO_2 experiment but is only about 0.5°C warmer than was found when CO_2 was reduced to 40 ppm. *Hansen et al.* [1984] showed that the overall effects of greenhouse gas forcing and solar forcing are qualitatively comparable, since they both trigger essentially the same feedback mechanisms in the tropics and at high latitudes. This is illustrated by the results from the solar reduction run and the 40 ppm CO_2 simulation, which are exceptionally similar (compare Figure 5, Maps 7 and 8). Both simulations have similarly large reductions of atmospheric water vapor, resulting in less radiative warming from the atmospheric greenhouse effect. Both, also, experience substantial increases in ground albedo, due to growing amounts of sea ice and snow, and have planetary albedos that are further accentuated by increased low level clouds (see Table 2).

Considering that the theoretical and empirical basis for some amount of solar reduction is quite firm and that CO_2 fluctuations are likely (though the minimum level is not known), the large cooling effects created by these two forcings does begin to shape a possible climate scenario in which mid- and low-latitude Varanger glaciation may have been present. None of the forcings explored so far could have, by themselves, produced substantial glaciation on the lowest latitude continents. But the cooling generated by these climate forcings does indicate that a combination of forcings may in fact yield an ice age climate that would corroborate low-latitude Varanger glacial deposits.

Notably, both the 50% increase and 50% decrease in ocean heat transports resulted in decreased global mean temperatures for a world with Varanger-type paleogeography (Table 2), although the character of the cooling differs considerably between the two experiments (Figure 7a). The greater global mean cooling was associated with decreased ocean heat transports (-6.7°C in $\text{OHT}_{0.5}$ vs. -2.9°C in $\text{OHT}_{1.5}$), and resulted from a reduced energy flux into the mid- and high

latitudes that allowed sea ice to expand (compare Maps V, 3 and 6 in Figure 6). The expansion of sea ice reduced open ocean area, which in turn reduced the amount of water vapor transferred to the atmosphere (Figure 7b). It also created a platform for additional snow accumulation, further increasing the surface albedo by nearly 5 percent. Additionally, decreased ocean heat transports led to greater low-level cloud cover (+5.5%) and a slight decrease in high clouds, both of which enhance cooling. Cloud cover in OHT_{0.5} actually decreased poleward of 50°, where the extra sea ice (less open water) tended to stabilize the air column. However, mid- and low-latitude cloud coverage was greater (Figure 7c) since tropical convection was more active (a result of the less efficient tropical heat removal) and because atmospheric eddies became more energetic in compensation for decreased energy transport in the oceans.

In contrast, tropical cooling dominated the temperature signal (Table 2 and Figure 7a) when ocean heat transports were increased (-8.6°C in OHT_{1.5} vs. -2.5°C in OHT_{0.5}). Under these conditions, more efficient removal of heat from the tropics resulted in weakened tropical convection, a less effective water vapor feedback (Figure 7b), and relatively less cloud cover (Figure 7c), particularly in mid-latitudes. Initially, increased heat transports from the tropics also warmed the mid- to high latitudes more effectively, melting the sea ice margins further back than in the reduced ocean heat transport scenario. Ultimately, however, the greater exposure of ocean surface increased atmospheric instability at high latitudes, generating more cloud cover that affected the global mean planetary albedo in a manner very similar to that of the increased sea ice cover in the reduced ocean heat transport scenario.

Increasing the obliquity to 60° dramatically altered the meridional temperature gradient of the planet, since the hemispheres experienced extreme ranges of seasonal solar insolation. The obliquity experiment was the only simulation that became unstable before reaching an equilibrium state. However, the cause of the instability is informative in this case, as it resulted from an over-thickening of the sea ice in certain grid cells of the GCM (that is, ice thickness exceeded our model's imposed maximum mixed-layer of 100 meters). Northern Hemisphere air temperatures are moderated by the ocean-dominated environment, thus they change only 15°C from summer to

winter in this simulation. In sharp contrast, the ground temperatures over the landlocked south pole fluctuate seasonally from a monthly average as low as -31°C in July to a boiling (literally) 104°C in January. The tropical temperature range was everywhere less than 7°C during the annual cycle, and was less than 2°C over most areas. Nowhere on the planet were there regions that remained below 0°C year round; however, a swath between 15°N and 15°S experienced annual average temperatures of less than 10°C (Table 2 and Figure 5, Map 9).

While these initial results are supportive of obliquity's potential for generating low-latitude cooling, we must reiterate that this run became unstable after only 6 simulated years. At the time, both negative and positive feedback mechanisms were still competing. Global annual average SSTs barely changed at all, yet atmospheric water vapor declined by over 40% as a result of dramatically altered atmospheric dynamics. Despite the water vapor drop-off, which tends to cool the climate, other climate components tending to warm the climate also changed. For example, cloud cover, sea ice, and snow cover, all decreased causing a steep decline in the planetary albedo.

4.2. Surface Air Temperature Response to Combined Forcings

Combining climate forcing mechanisms is a non-additive process since each of the forcings, to some extent, trigger the same basic feedback mechanisms. In most of the cooler experiments sea ice and snow cover expand, along with the associated albedo feedback. Water vapor levels in the atmosphere decline, reducing the overall greenhouse effect. Still, the effect of more than one forcing does tend to be greater than that of individual forcings and it is certainly possible, if not likely, that multiple climate forcings acted in conjunction during the Varanger interval. We conducted six simulations that combined two or more forcings. In addition to the experiments that combined 4 times carbon dioxide levels with solar forcing and, separately, with decreased ocean heat transports we ran the following combinations that caused significant cooling: decreased solar luminosity with decreased ocean heat transport, decreased CO_2 (140 ppm) with decreased solar luminosity, and two combinations with decreases of all three forcings: -6% solar luminosity, 140 ppm CO_2 , $\text{OHT}_{0.5}$, as well as -6% solar luminosity, 40 ppm CO_2 , and $\text{OHT}_{0.5}$.

We first tested the hypothesis that high greenhouse gas levels, suggested for other intervals of the Neoproterozoic, persisted throughout the Varanger ice age. In such scenarios it would be necessary to show that other forcings could more than offset the warming generated by the enhanced greenhouse effect. Our results give no indication of this having been the case, even when we added other forcings that individually cooled the climate. Reduced ocean heat transports combined with the 1260 ppm CO₂ yielded tropical temperatures that still exceeded 36°C and decreased the global greenhouse warming by only 3.5°C (Table 2 and Figure 5, Map 2). Solar luminosity, when reduced along with the increased CO₂, was somewhat more effective. However, the faint sun, which individually produces dramatic cooling, is still almost fully offset by the CO₂ (Table 2 and Figure 5, Map 4). Such results would lead us to believe that at least some reduction in CO₂ (or another greenhouse gas) from the hypothesized higher Neoproterozoic levels is a prerequisite to glacial initiation at low latitudes in the Varanger.

The combination of 6% solar luminosity decrease and halving ocean heat transports cooled the global average temperature to a frigid -13.3°C, with tropical temperatures dropping to 7°C (Table 2 and Figure 5, Map 10). The surface air temperature field was found to vary less with longitude when ocean heat transports were decreased (see Figure 5, Maps 2, 3, 10, 12, 13) because the meridional influence of the ocean fluxes is less. The resulting pattern shows broader cooling throughout the mid-latitudes. Combining the 6% lower solar luminosity with a 140 ppm CO₂ level gave even cooler tropical temperatures (6.4°C at 4°N), but was more than 5°C warmer in the global average than in the OHT_{0.5}/Solar decrease simulation. Water vapor and albedo feedbacks were both weaker overall with the CO₂/Solar decrease and, although low cloud amounts are also greater in the first combination (OHT_{0.5}/Solar), the albedo increase appears to be dominated by surface changes (Table 2).

It is important to note that the above result (OHT_{0.5} combined with reduced solar flux presents a larger impact than that caused by the 140 ppm CO₂/Solar decrease combination) would not have been an obvious conclusion were we to assume that the effects of individual forcings were simply additive. In fact, the results of the individual forcing experiments would lead us to

expect the opposite. As mentioned previously, the fact that CO₂ and solar radiation trigger comparable feedbacks, with greatest impact in the tropics, makes their combined climate influence less than when solar decrease is allied with the altered ocean flux, which has a greater high-latitude influence. We did not run a simulation combining reduced CO₂ with OHT_{0.5} (with modern solar luminosity), but we expect that combination would also yield greater cooling than the CO₂ /solar combination, for similar reasons.

Not surprisingly, the largest cooling occurred when CO₂, solar luminosity and ocean heat transports were all combined (Figure 5, Maps 12 and 13). We ran two such simulations. Both runs included the same degree of reduction in solar luminosity (-6%) and ocean heat transport (-50%), but differed by the amount of atmospheric CO₂ decrease: one simulation used 140 ppm CO₂ and the other 40 ppm. Global annual mean surface air temperature declines to -17.1°C when the CO₂ level is dropped to 140 ppm (Figure 5, Map 12). That is 3.8°C cooler than the run that did not include a change in atmospheric CO₂ (Figure 5, Map 10; CO₂ level = 315 ppm), indicating that the sensitivity to the CO₂ decrease is much smaller if it is changed in combination with other forcing reductions. As mentioned above, this underscores the point that each of the forcings operates, to some extent, by triggering similar feedback. Therefore, the individual responses are not linearly additive. Resulting tropical temperatures were still above freezing on the annual average with the combination of OHT_{0.5}/-6% Solar/140 ppm CO₂. Annual average temperatures near the equator hover around 4°C throughout the year in that simulation, and they are not found to be below-freezing equatorward of 20°N and 12°S at any longitude. All continents do, however, experience some areas of below freezing annual average temperatures, with the single exception of Tibet.

With CO₂ further decreased to 40 ppm, in combination with the other two forcings, global annual average temperatures dropped below -20°C and zonally averaged annual tropical temperatures were below freezing (-1°C), the only one of our scenarios to show such a result (Table 2). Over the continents temperatures are well below freezing at all latitudes, and are only above 0°C in two narrow bands, both of which lie over open ocean along the equator (Figure 5, Map 13).

4.3. *Snow and Ice Accumulation On Land*

The GCM explicitly calculates snow fall and melting rates, producing snow coverage and depth diagnostics, which we use to evaluate the potential for glacial initiation over the continents. Having no dynamic ice-sheet component, snow accumulation at mid to high latitudes does not encroach laterally upon lower latitudes, regardless of the accumulation totals. However, high albedo snow cover at mid and high latitudes is a powerful positive feedback to cooling that makes conditions more favorable for in situ, low-latitude, glacial initiation.

The areal extent of snow and ice cover roughly corresponds to the location of the annual average zone of subzero temperatures (compare corresponding maps in Figures 5 and 6). The snow and ice extent shows little change resulting from the paleogeographic changes alone. Yet snow depths are much greater with the Varanger paleogeography than in the modern climate simulation (Table 2) because a greater proportion of land lies at high latitudes in the Varanger reconstruction.

Continental snow cover in the increased CO₂ simulations is reduced by as much as 70% compared with simulations containing modern CO₂ levels, which is the case despite a hydrological cycle that is 38% stronger overall (as measured by precipitation/evaporation rates) and nearly 55% stronger over land. The warming in these simulations simply leaves too few regions at or below freezing, thus most precipitation falls as rain rather than snow. Perhaps more moderate increases of CO₂ could lead to more snow accumulation by strengthening the hydrological cycle without raising high-latitude temperatures beyond the freezing point. However, previous doubled-CO₂ experiments using the GISS GCM and modern geography do not support such hypotheses.

In the Varanger simulations, the general trend is for continental snow and ocean ice cover to increase as global temperature declines (Figure 8). Surface air temperature and snow depth (accumulation during the 60-year simulation period) are not, however, similarly correlated. Snow depths increase with decreasing temperature for simulations with mean annual surface air temperatures above 10°C. However, the depth versus temperature trend is reversed in runs with global mean temperatures below 0°C (Figure 8). This effect is almost certainly related to the decline

in open ocean surface waters, which are increasingly covered by sea ice in the colder climate scenarios (Figure 6). As sea ice extent increases, the transfer of moisture into the atmosphere is reduced and convective activity over land becomes less vigorous, both of which serve to reduce precipitation rates and snow accumulation. Naturally, the negative correlation between ocean ice cover and snow cover reverses at very warm temperatures (e.g. simulations 1, 2 and 9) because precipitation is mostly in the form of rain and the rate of snow accumulation is overwhelmed by even more rapid ablation rates.

The coldest Varanger simulations reveal that certain combinations of climate forcings can cause snow and ice to begin accumulating on land in the tropics. In none of our scenarios do we find that the planet becomes completely ice-covered, though annual average sea ice extends into the tropics in the more extreme cooling simulations. Two of the coldest simulations that rely on solitary forcings, decreased solar luminosity and reduction of CO₂ to 40 ppm, push the snow and ice margin into the tropics at specific longitudes (Figure 6, Maps 7 and 8). Neither of these experiments, however, maintains snow on the tropical continents throughout the year. Combining forcings in pairs pushes the entire ice margin equatorward at all longitudes, but still does not accumulate significant snow amounts on tropical land masses (Figure 6, Maps 10 and 11). However, the combination of CO₂ reduction, solar radiation decrease, and decreased ocean heat transports (Figure 6, Maps 12 and 13) extends snow and ice into the tropics of both hemispheres and shows the first significant signs that snow is accumulating across the low-latitude continents, including Australia. In the coldest experiment (Figure 6, Map 13) large accumulations of snow and ice cover tropical land regions. In all of our simulations, the equatorial oceans remain uncovered by sea ice, thus evaporation was able to continue providing the atmospheric moisture necessary for the growing tropical “ice sheets.” Recall that this tropical thickening of the snow on land occurs despite the global average decline in the depth of the snow pack as temperatures got colder (Table 2). So, in the coldest scenarios, the low-latitude snow depth begins to increase while the higher latitude snow depth decreases compared to runs that are, globally, somewhat warmer.

The behavior of the 60° obliquity simulation bears special mention, in large part because of the qualitative uniqueness of the results compared with the other experiments, all of which tend to differ mostly quantitatively. Globally snow cover, snow depth, and sea ice extent are minimal in this experiment (Table 2 and Figure 6, Map 9). Despite the fact that the simulation did not reach equilibrium the trend towards declining snow cover is so extreme after just 6 years (the simulation begins with nearly 30% snow coverage and drops to almost 0%) that we feel confident in interpreting these results as strongly arguing against increased obliquity as a sole cause of low-latitude Varanger glaciation. The extreme warm temperatures experienced over land during summer are simply too great to sustain snow cover year round. The cooler ocean temperatures arising under the high obliquity conditions further complicate the potential for ice sheet initiation because they reduce evaporation. Thus, atmospheric moisture content and precipitation drop as well. The low latitudes are particularly dry, more so than in other Varanger experiments, reducing the chance for large accumulations of snow on tropical continents; significant accumulations would be required to overcome the tropical temperatures which, though cool, are continuously above the melting point.

In each of the coldest experiments snow depths continued to increase over land well after temperatures reached an equilibrium state. Does this imply that glaciers would have begun to form in these experiments? It is difficult to say without incorporating a dynamic ice sheet into a global climate model. Ice sheets cannot be appropriately simulated by the simple accumulation of snow as calculated in a GCM. Furthermore, though the GISS GCM can continue to accumulate snow indefinitely if temperature and moisture conditions dictate, the model does not have the ability to simultaneously alter the topography. Most of the cold Varanger simulations have certain regions where snow accumulates to depths measured in the tens of meters. If we could run a GCM simulation long enough (thousands of years) we would find, at some point, that the rising elevation of the surface becomes a dominant factor in the evolution of the ice sheet and of the global climate. Modern Antarctica is a cold, dry desert partly because its surface sits thousands of meters above sea level, and the Laurentide ice sheet of the last glacial maximum actually altered the flow of the jet stream in the Northern Hemisphere, disrupting climate patterns throughout the

world [Kutzbach and Guetter, 1986; Kutzbach *et al.*, 1989; Ruddiman *et al.*, 1989]. Our ability to tackle such feedbacks using a GCM will require longer integrations and improved land ice formulations.

5. DISCUSSION

These Varanger simulations show that there do exist combinations of climate forcings that are capable of cooling global temperatures to the point where snow accumulates on low-latitude continents. Whether or not the scenarios we have used are justifiable depends on a number of items: the reality of the altered forcing mechanisms, the GCM's ability to simulate critical components of the climate system, the quality of Varanger paleogeographic reconstructions, and the interpretation of geologic data used to verify simulation results.

One potentially important paleogeographic climate effect not explored in our scenarios is the effect of orography on the continental climates; recall that we assigned a uniformly low topography to our continents for these simulations. Glacial initiation would have been aided by the presence of high-elevation mountain ranges and plateaus, as it was in the Cordilleran, Himalayan and Andean ranges during the Pleistocene, and as *Jenkins and Frakes* (1998) found in their idealized-continent Neoproterozoic simulations. Prominent mountain ranges created by Pan-African orogenic activity may well have existed in mid- to high latitudes during the Varanger glacial interval. Further experiments using realistic paleotopography are certainly warranted.

5.1 Ocean Heat Transport Distributions

Ocean heat transports during the Varanger glacial interval would certainly have been different than at present, given the significantly altered ocean basin configuration of that time. Determining exactly how these transports differed from the modern is a difficult proposition, though, since there are many possible distributions other than the ones we employed that could influence global and tropical climates in unexpected ways. Comparisons between individual GCMs are further complicated by the differing techniques used to parameterize key elements of the models. One readily apparent example of this is the dramatically different ocean basin configuration used in this study (i.e., Varanger paleogeography) compared to other recent Neoproterozoic

climate simulations (e.g., the idealized rectangular supercontinent of *Jenkins and Frakes* [1998] and *Jenkins and Smith* [1999]). Perhaps more importantly, individual GCMs adopt different approaches to the parameterization of meridional ocean heat flux. For example, we derive fluxes using the GISS GCM and specified SSTs [*Russell et al.*, 1993]; other models use observations to estimate a zonally-averaged meridional ocean heat transport. In addition, nearly all models tune the ocean heat fluxes to better simulate modern SST distributions, sea ice extent and interannual variability. Such tuning is justifiable to a certain degree, as the fluxes are poorly constrained by observations. However, such variable approaches to the parameterization of ocean heat fluxes introduces the possibility of considerable model-to-model differences in experimental results. Future comparison between models, running experiments with identical boundary conditions, will add confidence to conclusions regarding the effects of ocean heat transports on Neoproterozoic climates.

At present, we can draw some first-order comparisons between the ocean heat transport experiments in this study, another Neoproterozoic study that employed the GENESIS GCM [*Jenkins*, 1999], and a previous GISS GCM sensitivity experiment [*Rind and Chandler*, 1991]. All of these simulations found an inverse correlation between sea ice extent and ocean heat transport change. They also show that tropical temperatures cool when ocean heat transports are increased and that global cooling, dominated by mid- to high-latitude temperature change, occurs when transports decline. Our OHT_{1.5} simulation differs from the other studies in that global mean temperatures decline slightly, whereas other simulations yielded overall warming. This discrepancy is the result of small, but important, differences in the zonal distribution of ocean heat transports used in the various experiments. *Rind and Chandler's* [1991] simulations used an altered ocean heat transport scenario that preferentially increased transports near sea ice margins. The result was a dramatic reduction of sea ice, which triggered positive feedbacks that enhanced warming (e.g. albedo decrease, water vapor increase); warming occurred at all latitudes but was primarily a high-latitude phenomenon. Conversely, the Varanger OHT_{1.5} transports were increased by the same factor at all latitudes. Maximum absolute changes were in the lower and middle latitudes, which

severely limited the tropical water vapor feedback (see Figure 7b, above) causing a cooling that dominated the global signal. *Jenkins'* [1999] “increased” transport scenario, like ours, also shows a slight cooling tendency in the tropics (see his figure 8). We speculate that a larger ocean heat transport increase in that model would further reduce tropical water vapor amounts, eventually dominating the sea ice feedback, as it does in our simulations.

Comparisons of the Varanger experiments with the GENESIS simulations are made a bit confusing by certain semantic issues: Compared to estimates of modern ocean heat transports [*Carrissimo et al.*, 1985; *Trenberth and Solomon*, 1994; *Zhang and Rossow*, 1997], the GENESIS model’s current climate transports are too low by a factor of three to six, while the GISS GCM control transports are slightly high. *Jenkins* [1999] “increased” transport scenario (Qfact3 in his paper) used lower levels of ocean heat transport than did our Varanger scenario OHT_{1.0}, and his Qfact1 scenario, which used ocean heat transports that were similar in magnitude to a modern climate GENESIS control run, were less even than our reduced scenario (OHT_{0.5}). Thus, the terms “increased” and “decreased” are relative to the specific GCM in question.

Finally, the fact that both increased (OHT_{1.5}) and decreased (OHT_{0.5}) ocean heat transports led to global cooling does not necessarily imply that the modern ocean heat transport scenario (OHT_{1.0}) gave the optimal warming for the Varanger interval. It does suggest, however, that the optimum for the Varanger paleocean configuration lies somewhere between 50% and 150% of modern values.

5.2. Are Important Atmospheric CO₂ Feedbacks Missing From GCMs?

Altered levels of atmospheric CO₂ had a large influence on global climate in the Varanger simulations. Although lowered solar insolation and altered ocean transports may also be necessary to achieve tropical glaciation, fluctuating levels of CO₂ (and perhaps other greenhouse gases) are probably the only mechanism, of those explored in these simulations, that would be capable of transitioning the Varanger climate between glacial and ice-free states over geologically short periods of time.

One other potentially significant feedback mechanism, related to the role of atmospheric carbon dioxide in very cold climates, was not considered in these simulations. Surface air temperatures characteristically fall below -80°C in some of the colder Varanger simulations. Carbon dioxide condensation, at standard mean sea level pressure, could potentially commence at these temperatures, dependent somewhat on the local atmospheric pressure and partial pressure of atmospheric CO_2 . Under conditions of extreme climate forcing, such as low solar luminosity, decreased greenhouse gases, reduced ocean heat transport, etc., further reduction in atmospheric carbon dioxide may have occurred through the process of condensation. This, of course, occurs on a seasonal basis on Mars and plays a significant role in that planet's ancient and present day climate [Kasting, 1991; Forget *et al.*, 1998]. However, CO_2 is the major constituent in the martian atmosphere, whereas it is a trace component (admittedly an important one) of Earth's atmosphere.

Carbon dioxide condensation and cloud formation may also have played a role in the Varanger climate system. As with water clouds, the role of CO_2 clouds would depend greatly on details of their formation; particle size, cloud height, diurnal variation, latitudinal distribution and optical thickness all alter the global radiative effect of clouds. Previous studies have suggested that the role of CO_2 clouds in early Earth climates may have had either a warming or cooling influence [Caldeira and Kasting, 1992; Forget and Pierrehumbert, 1997] depending upon the above characteristics. Most general circulation models of the Earth's atmosphere do not incorporate CO_2 condensation physics and, therefore, the Neoproterozoic studies using GCMs have not included this feedback mechanism. Further exploration of this issue is warranted and could produce a better accounting of extremely cold climates such as the Varanger ice age.

5.3 Obliquity

Obliquity, by itself, appears to be incapable of accounting for Varanger ice sheet formation. This conclusion, however, is based on a lone simulation using that forcing. Our experiments are incomplete in this area, and we point out that our model results using the GISS GCM differ from those of Oglesby and Ogg [1999] who used the NCAR CCM1 climate model (albeit with modern geography) to explore the effects of increased obliquity on climate. It is important to note that

although the concept of a large obliquity for the Earth ~600 Ma is intriguing and has received serious consideration from the Neoproterozoic scientific community [e.g., *Williams et al.*, 1998], it is basically a theoretical model for ice distribution that does not stand up to the geological evidence at hand; for example, the high obliquity model cannot explain how the Earth could have oscillated between the cold glacial and the warm interglacial intervals preserved in the stratigraphic record. Geophysical considerations of the evolution of Earth's obliquity also suggest that the obliquity angle is fairly robust, with a tendency perhaps to increase rather than decrease with time [Ward, 1982; Laskar *et al.*, 1993; Rubincam, 1995]. Future experiments that combine other forcing factors with smaller decreases in obliquity, rather than with large increases, may help clarify what role obliquity plays, if any, in long-term climatic trends.

5.4 Implications for the Snowball Earth Hypothesis

The "snowball Earth" hypothesis has garnered much attention recently as an explanation for low-latitude glaciations in the Neoproterozoic record [Kirschvink, 1992; Hoffman *et al.*, 1998], as well as related phenomena such as the large negative carbon isotope excursions (as much as -5‰) found in cap carbonates overlying Neoproterozoic glacial deposits worldwide. One significant aspect of the snowball Earth hypothesis, as presented by Hoffman *et al.* [1998], is that the Earth's oceans were entirely cut off from the atmosphere for as much as 9 million years during the mid-Neoproterozoic Sturtian glacial interval. Though our focus here was low-latitude snow accumulation on continents, and not tropical sea ice growth, our results do allow us to offer some comments regarding the viability of a snowball Earth scenario for the late Neoproterozoic Varanger glacial interval.

As noted above, only the most extreme scenarios in our study yielded tropical conditions conducive to glaciation. Yet, even under these conditions, sea ice never completely covered the tropical ocean (Figure 6, Maps 12 and 13); as much as 30% of the ocean waters remained ice-free, even with CO₂, solar luminosity and ocean heat transports all reduced. Our simulations suggest, therefore, that low-latitude continental glaciation may be easier to accommodate with a combination of climate forcing mechanisms than global ocean ice cover might be. We recognize that the roles of

ocean circulation changes and other greenhouse gases (e.g. methane) have yet to be explored in detail, so there may well exist alternate Varanger boundary conditions that would lead to greater sea ice coverage in the GISS GCM.

Our results are distinct from those of *Jenkins and Smith* [1999], who found that global sea ice coverage was achieved using extreme forcings and an idealized, equator-straddling continent in the GENESIS GCM (see their figure 3c). In their experiments, tropical cooling would have been promoted by the decreased ratio of low-latitude ocean to land, which probably increased tropical surface albedo and decreased the water vapor feedback in comparison with our simulations using the Varanger paleogeography. Differences between the GISS and GENESIS GCM results appear to be more substantial than would be expected based on the boundary conditions alone, but any quantitative comparison would be precarious without more analogous simulations. Eventually, the role of the oceans in extremely cold climates should be explored using fully dynamic ocean-atmosphere-sea ice models, something that will require significant computational resources, and further advancements in GCMs. Model-model comparisons may prove as informative as model-data comparisons, at this point, and a series of identical experiments using different climate models would probably offer substantial insight into the climate processes at work during the Neoproterozoic.

At present, no GCM is fully capable of exploring the details of a runaway icehouse effect; thus much of the current debate will remain rooted in evidence from the geologic record. Our inability to model all aspects of the snowball Earth hypothesis does not, however, invalidate a GCM approach to understanding Neoproterozoic climate processes, nor does it prevent a more qualitative evaluation of the hypothesis on geological or climatological grounds. For example, a key problem for the snowball Earth hypothesis concerns an unresolved discrepancy between geologic evidence and the climatic processes the hypothesis invokes: How can a total shutdown of the hydrologic cycle be reconciled with the need for active, wet-based continental ice sheets to produce the low-latitude glacial deposits?

6. CONCLUSIONS

Modulation of individual climate forcings is insufficient for the initiation of low-latitude continental ice sheets in the late Neoproterozoic Varanger glacial interval. A realistic paleocontinental reconstruction for that time period provides an important boundary condition to help constrain the role of climate forcings in the initiation of Neoproterozoic glaciation. However, Varanger paleogeography alone does not produce the low surface air temperatures or snow accumulation rates required to initiate low-latitude glaciation; on the contrary, the global average temperature is about 1°C warmer in the Varanger simulation than in a modern climate control run. Average snow depths increase on land, but the equatorward extent of snow does not. Decreased solar luminosity as a forcing mechanism during the Neoproterozoic provides a cooling effect, as expected, but its slow rate of change cannot account for the higher frequency climate fluctuations observed in the geologic record. Other climate forcings considered individually – reduction of atmospheric CO₂ to 140 ppm (or 40 ppm), increased or decreased ocean heat transports, and altered obliquity – also do not yield the coinciding surface air temperature and snow fall rates that would allow snow to accumulate on low-latitude continents.

Combinations of forcings are more effective in producing conditions amenable to the development of low-latitude ice sheets. Paired climate forcing combinations do not necessarily produce additive results because each forcing, to some degree, triggers similar feedback mechanisms. However, forcing combinations did result in further cooling of the planet, extending the annual average freeze line, as well as snow and ice accumulations, into the marginal tropics. The lower solar luminosity and 40 ppm CO₂ simulations indicate that snow and ice accumulations in mid-latitudes could have occurred during the Varanger glacial interval if either of those forcings mechanisms were, in fact, realized. Simulations which combine decreased ocean heat transports with the CO₂ and solar radiation reductions reveal that snow accumulation on Australia and other low-latitude land areas is a definite possibility given large, and perhaps not unrealistic, changes in climate forcing levels for the Neoproterozoic. None of the Varanger climate simulations suggest that it is possible to have generated low-latitude glaciation without coeval glacial conditions existing

at higher latitudes. In fact, in all scenarios except the increased obliquity simulation, glaciation at high and mid-latitudes would have preceded low-latitude ice sheet buildup. The distribution of glacial deposits throughout the southern hemisphere supports the model's results, but the uncertain dating of glacial deposits means we cannot completely rule out the possibility that the Varanger ice age consisted of multiple events, not all of which were as severe as the event that glaciated Australia.

This particular assemblage of climate forcing scenarios was specifically aimed at exploring the potential for snow and ice accumulation on the continents, and does not necessarily affirm or deny the possibility of a "snowball Earth" scenario during the Neoproterozoic. The GISS GCM results suggest that capping the oceans would require yet more extreme forcings than were tested in this study; however, as snowball Earth conditions were found to occur in another GCM, detailed model/model comparisons may be needed to distinguish model biases from true climatological effects. We note that continental ice sheet growth would halt under any scenario that led to global sea ice cover, as the atmosphere's only significant source of moisture – the ocean – would be cut off.

Acknowledgements. The authors wish to acknowledge numerous helpful discussions with N. Christie-Blick and D. Rind, as well as the useful suggestions of three anonymous reviewers. The MapProjector software for transforming paleogeographic maps into GCM boundary conditions was written by M. Shopsin. Support was provided by NSF grants ATM-93-20372 and ATM-99-07640 (MC and LS), EAR-94-18294 (LS), by the NASA Climate Program and NASA Cooperative Agreement NCC5-328 (MC and LS), and the Lamont-Doherty Center for Climate Research (LS).

REFERENCES

- Baker, J. D., Jr., Ocean dynamics and energy transfer: some examples of climatic effects, in *National Research Council Geophysics Study Committee, Energy and Climate. Studies in Geophysics Series*, pp. 121-127, Natl. Acad. of Sci., Washington, D.C., 1977.
- Barron, E.J., W.H. Peterson, D. Pollard, and S. Thompson, Past climate and the role of ocean heat transport: model simulations for the Cretaceous, *Paleoceanography*, 8, 785-798, 1993.
- Beck, J.W., R.L. Edwards, E. Ito, F.W. Taylor, J. Recy, F. Rougerie, P. Joannot, and C. Henin, Sea-surface temperature from coral skeletal strontium/calcium ratios, *Science*, 257, 634-647, 1992.
- Bennett, M.R., P. Doyle, A.E. Mather, and J.L. Woodfin, Testing the climatic significance of dropstones: An example from southeast Spain, *Geol. Mag.*, 131, 845-848, 1994.
- Berner, R.A., A model for atmospheric CO₂ over Phanerozoic time, *Am. J. Sci.*, 291, 339-376, 1991.
- Berner, R.A., GEOCARB II: A revised model of atmospheric CO₂ over Phanerozoic time, *Am. J. Sci.*, 294, 56-91, 1994.
- Biju-Duval, B. and O. Gariel, Nouvelles observations sur les phénomènes glaciaires "éocambriens" de la bordure nord de la synéclyse de Taoudeni, entre le Hank et le Tanezrouft (Sahara occidental), *Palaeogeogr. Palaeoclimat. Palaeoecol.*, 6, 283-315, 1969.
- Bowring, S.A., and D.H. Erwin, A new look at evolutionary rates in deep time: Uniting paleontology and high-precision geochronology, *GSA Today*, 8, p. 1-8, 1998.
- Broecker, W.S. and G.H. Denton, The role of ocean-atmosphere reorganizations in glacial cycles, *Geochim. Cosmochim. Acta*, 53, 2465-2501, 1989.
- Bromham, L., Rambaut, A., Fortey, R., Cooper, A., and Penny, D., Testing the Cambrian explosion hypothesis by using a molecular dating technique: *Proceedings of the National Academy of Sciences*, 95, p. 12386-12389, 1998.

- Caldeira, K. and Kasting, J.F., 1992, Susceptibility of the early Earth to irreversible glaciation caused by carbon dioxide clouds: *Nature*, v. 359, p. 226-228.
- Canfield, D.E., and Teske, A., Late Proterozoic rise in atmospheric oxygen concentration inferred from phylogenetic and sulphur-isotope studies: *Nature*, 382, p. 127-132, 1996.
- Carissimo, B. C., Oort, A. H., and Vonder Haar, T. H., Estimating the meridional energy transports in the atmosphere and ocean: *J. Phys. Ocean.*, 15, p. 82-91, 1985.
- Carver, J.H., and I.M. Vardavas, Precambrian glaciations and the evolution of the atmosphere, *Ann. Geophys.*, 12, 674-682, 1994.
- Chandler, M.A., D. Rind, and R. Ruedy, Pangaeon climate during the Early Jurassic: GCM simulations and the sedimentary record of paleoclimate. *Geol. Soc. Am. Bull.*, 104, 543-559, 1992.
- Christie-Blick, N., Glacial-marine and subglacial sedimentation, upper Proterozoic Mineral Fork Formation, Utah, in *Glacial-marine Sedimentation*, edited by B.F. Molnia, pp. 703-776, Plenum Press, New York, 1983.
- Chumakov, N.M. and D.P. Elston, The paradox of late Proterozoic glaciations at low latitudes, *Episodes*, 12, 115-120, 1989.
- Conway Morris, S., The fossil record and the early evolution of the Metazoa: *Nature*, 361, p. 219-225, 1993.
- Covey, C., Climate change: Credit the oceans? *Nature*, 352, 196-197, 1991.
- Covey, C. and E.J. Barron, The role of ocean heat transport in climatic change, *Earth-Sci. Rev.*, 24, 429-445, 1988.
- Cowie, J.W., Ziegler, W., and Remane, J., Stratigraphic Commission accelerates progress, 1984 to 1989: *Episodes*, 12, p. 79-83, 1989.
- Crowell, J.C., Ice ages recorded on Gondwanan continents, *Trans., Geol. Soc. S. Africa*, 86, 238-261, 1983.
- Crowley, T.J. and S.K. Baum, Effect of decreased solar luminosity on Late Precambrian ice extent, *J. Geophys. Res.*, 98, 16,723-16,732, 1993.

- Dalziel, I.W.D., Pacific margins of Laurentia and East-Antarctica as a conjugate rift pair: Evidence and implications for an Eocambrian supercontinent, *Geology*, *19*, 598-601, 1991.
- Dalziel, I.W.D., Neoproterozoic-Paleozoic geography and tectonics: Review, hypothesis, environmental speculation, *Geol. Soc. Am. Bull.*, *109*, 16-42, 1997.
- Deynoux, M., Periglacial polygonal structures and sand wedges in the late Precambrian glacial formations of the Taoudeni Basin in Adrar of Mauritania (West Africa), *Palaeogeogr. Palaeoclimat. Palaeoecol.*, *39*, 55-70, 1982.
- Deynoux, M., G. Kocurek, and J.N. Proust, Late Proterozoic periglacial eolian deposits on the west African platform, Taoudeni Basin, western Mali, *Sedimentology*, *36*, 531-549, 1989.
- Edwards, M.B., Sedimentology of the Upper Proterozoic glacial record, Vestertana Group, Finnmark, north Norway, *Nor. geol. unders. Bull.* *394*, 76 p., 1984.
- Elming, S.-Å., L.J. Pesonen, M.A.H. Leino, A.N. Khramov, N.P. Mikhailova, A.F. Krasnova, S. Mertanen, G. Bylund, and M. Terho, The drift of the Fennoscandian and Ukrainian shields during the Precambrian: A palaeomagnetic analysis, *Tectonophysics*, *223*, 177-198, 1993.
- Embleton, B.J.J. and G.E. Williams, Low palaeolatitude of deposition for late Precambrian periglacial varvites in South Australia: Implications for palaeoclimatology, *Earth Planet. Sci. Lett.*, *79*, 419-430, 1986.
- Evans, D.A., Geochronological and paleomagnetic constraints upon the Neoproterozoic climatic paradox, *American Journal of Science*, in press.
- Fairchild, I.J., M.J. Hambrey, B. Spiro, and T.H. Jefferson, Late Proterozoic glacial carbonates in northeast Spitsbergen: New insights into the carbonate-tillite association, *Geol. Mag.*, *126*, 469-490, 1989.
- Forget, F. and R.T. Pierrehumbert, Warming Early Mars with Carbon Dioxide Clouds That Scatter Infrared Radiation, *Science*, *278*, 1273-1276, 1997
- Forget, F., F. Hourdin, and O. Talagrand, CO₂ snowfall on Mars: Simulation with a general circulation model, *Icarus*, *131*, 302-316, 1998.

- Girdler, R.W., The palaeomagnetic latitudes of possible ancient glaciations, in *Problems in Palaeoclimatology, Proceedings of NATO Paleoclimates Conference*, edited by A.E.M. Nairn, pp. 115-118, Interscience Publishers, New York, 1964.
- Gough, D.O., Solar interior structure and luminosity variations, *Solar Phys.*, 74, 21-34, 1981.
- Grotzinger, J.P., Bowring, S.A., Saylor, B.Z., and Kaufman, A.J., Biostratigraphic and geochronologic constraints on early animal evolution: *Science*, 270, p. 598-604, 1995.
- Guilderson, T.P., R.G. Fairbanks, and J.L. Rubenstone, Tropical temperature variations since 20,000 years ago: modulating interhemispheric climate change, *Science*, 263, 663-665, 1994.
- Hagstrum, J.T., R. Van der Voo, B. Auvray, and N. Bonhommet, Eocambrian-Cambrian paleomagnetism of the Armorican Massif, France: *R. Astron. Soc. Geophys. J.*, 61, 489-517, 1980.
- Hambrey, M.J., *Glacial Environments*, UCL Press, London, 292 p., 1994.
- Hambrey, M.J., and Harland, W.B., eds., *Earth's Pre-Pleistocene Glacial Record: Cambridge, United Kingdom*, Cambridge University Press, 1019 p., 1981
- Hambrey, M.J., and Harland, W.B., The late Proterozoic glacial era: *Palaeogeography, Palaeoclimatology, Palaeoecology*, v. 51, p. 255-272, 1985.
- Hansen, J.E., I. Fung, A. Lacis, D. Rind, S. Lebedeff, R. Ruedy, G. Russell, and P. Stone, Global climate changes as forecast by Goddard Institute for Space Studies Three-Dimensional Model, *J. Geophys. Res.* 93, 9341-9364, 1988.
- Hansen, J. E., G. Russell, D. Rind, P. Stone, A. Lacis, S. Lebedeff, R. Ruedy, and L. Travis, Efficient three-dimensional global models for climate studies: Models I and II, *Month. Weath. Rev.*, 111, 609-662, 1993.
- Hansen, J.E., A. Lacis, D. Rind, G. Russell, P. Stone, I. Fung, R. Ruedy, and J. Lerner, Climate sensitivity: Analysis of feedback mechanisms, in *Climate Processes and Climate Sensitivity*, edited by J.E. Hansen and T. Takahashi, Geophysical Monograph Series 29, p. 130-163, American Geophysical Union, Washington, D.C., 1984.

- Harland, W.B., Critical evidence for a great Infracambrian glaciation, *Geol. Rund.*, 54, 45-61, 1964.
- Harland, W.B., and D.E.T. Bidgood, Palaeomagnetism in some Norwegian sparagmites and the late Pre-Cambrian ice age, *Nature*, 184, 1860-1862, 1959.
- Hartmann, W.K., and S.M. Vail, Giant impactors: Plausible sizes and populations, in *Origin of the Moon*, edited by Hartmann, R.J. Phillips, and G.J. Taylor, pp. 551-566, Lunar and Planetary Institute, Houston, 1986.
- Hoffman, P.F., Did the breakout of Laurentia turn Gondwanaland inside-out? *Science*, 252, 1409-1412, 1991.
- Hoffman, P.F., A.J. Kaufman, G.P. Halverson, and D.P. Schrag, A Neoproterozoic snowball Earth, *Science*, 281, 1342-1346, 1998.
- Hofmann, H.J., Narbonne, G.M., and Aitken, J.D., Ediacaran remains from intertillite beds in northwestern Canada: *Geology*, 18, p. 1199-1202, 1990.
- Jenkins, G.S., Examining the sensitivity of Earth's climate to the removal of ozone, landmasses and enhanced ocean heat transport in the GENESIS global climate model, *Global and Planetary Change*, 20, 257-279, 1999
- Jenkins, G.S., and L.A. Frakes, GCM sensitivity test using increased rotation rate, reduced solar forcing and orography to examine low latitude glaciation in the Neoproterozoic, *Geophys. Res. Lett.*, 25, 3525-3528, 1998.
- Jenkins, G.S. and Smith, S.R., GCM simulations of snowball earth conditions during the late Proterozoic, *Geophys. Res. Lett.*, 26, 2263-2266, 1999.
- Karfunkel, J., and A. Hoppe, Late Proterozoic glaciation in central-eastern Brazil: Synthesis and model, *Palaeogeogr. Palaeoclimat. Palaeoecol.*, 65, 1-21, 1988.
- Kasting, J.F., Runaway and moist greenhouse atmospheres and the evolution of Earth and Venus, *Icarus*, 74, 472-494, 1988.
- Kasting, J.F., CO₂ condensation and the climate of early Mars, *Icarus*, 94, 1-13, 1991.

- Kasting, J.F., Proterozoic climates: The effect of changing atmospheric carbon dioxide concentrations, in *The Proterozoic Biosphere: A Multidisciplinary Study*, edited by J.W. Schopf and C. Klein, pp. 165-168, Cambridge University Press, Cambridge, United Kingdom, 1992.
- Kasting, J.F., Earth's early atmosphere, *Science*, 259, 920-926, 1993.
- Kasting, J.F., Warming Early Earth and Mars, *Science*, 276, 1213-1215, 1997.
- Kirschvink, J.L., Late Proterozoic low-latitude global glaciation: The snowball Earth, in *The Proterozoic Biosphere: A Multidisciplinary Study*, edited by J.W. Schopf and C. Klein, pp. 51-52, Cambridge University Press, Cambridge, United Kingdom, 1992.
- Knoll, A.H., Biological and biogeochemical preludes to the Ediacaran radiation, in *Origin and Evolution of Early Metazoa*: edited by Lipps, J.H., and Signor, P.W., New York, Plenum Press, p. 53-84, 1992a.
- Knoll, A.H., The early evolution of eukaryotes: A geological perspective: *Science*, 256, p. 622-627, 1992b.
- Knoll, A.H., and M.R. Walter, Latest Proterozoic stratigraphy and Earth history, *Nature*, 356, 673-678, 1992.
- Kröner, A., Non-synchronicity of late Precambrian glaciations in Africa, *J. Geol.*, 85, 289-300, 1977.
- Kröner, A., M.O. McWilliams, G.J.B. Germs, K.L. Schalk, and A. Reid, Paleomagnetism of late Precambrian to early Paleozoic magnetite-bearing formations in Namibia (southwest Africa): The Nama Group and Blaubeker Formation, *Am. J. Sci.*, 280, 942-968, 1980.
- Kutzbach, J.E., and P.J. Guetter, The influence of changing orbital parameters and surface boundary conditions on climate simulations for the past 18,000 years, *J. Atmos. Sci.*, 43, 1726-1759, 1986.
- Kutzbach, J.E., P.J. Guetter, W.F. Ruddiman, and W.L. Prell, Sensitivity of climate to late Cenozoic Uplift in southern Asia and the American West: *J. Geophys. Res.*, 94, 18393-18407, 1989.

- Laskar, J., F. Joutel, and P. Robutel, Stabilization of the Earth's obliquity by the Moon, *Nature*, 361, 615-617, 1993.
- Li Yianping, Li Yongan, R. Sharps, M.O. McWilliams, and Z. Gao, Sinian paleomagnetic results from the Tarim block, western China: *Precambr. Res.*, 49, 61-71, 1991.
- Li, Z.X., L. Zhang, and C.McA. Powell, South China in Rodinia: Part of the missing link between Australia-East Antarctica and Laurentia? *Geology*, 23, 407-410, 1995.
- Marshall, H.G., J.C.G. Walker, and W.R. Kuhn, Long term climate change and the geochemical cycle of carbon, *J. Geophys. Res.*, 93, 791-801, 1988.
- Matthews, E., Atlas of archived vegetation, land-use and seasonal albedo data sets: NASA Technical Memorandum 86199, National Aeronautics and Space Administration, Goddard Space Flight Center, Institute for Space Studies, 1985.
- McWilliams, M.O., and A. Kröner, Paleomagnetism and tectonic evolution of the Pan-African Damara Belt, southern Africa, *J. Geophys. Res.*, 86, 5147-5162, 1981.
- McWilliams, M.O., and M.W. McElhinny, Late Precambrian palaeomagnetism of Australia: The Adelaide Geosyncline, *J. Geol.*, 88, 1-26, 1980.
- Meert, J.G., and R. Van der Voo, The Neoproterozoic (1000-540 Ma) glacial intervals: No more snowball Earth? *Earth Planet. Sci. Lett.*, 123, 1-13, 1994.
- Meert, J.G., and R. Van der Voo, The assembly of Gondwana 800-550 Ma, *J. Geodynam.*, 23, 223-235, 1997.
- Miller, J. R., G.L. Russell, and T. Lie-Ching, Annual oceanic heat transports computed from an atmospheric model, *Dynam. Atmos. Oceans*, 7, 95-109, 1983.
- Moore, E.M., Southwest U.S.-East Antarctic (SWEAT) connection: A hypothesis, *Geology*, 19, 425-428, 1991.
- Morris, W.A., Paleolatitude of glaciogenic upper Precambrian Rapitan Group and the use of tillites as chronostratigraphic marker horizons, *Geology*, 5, 85-88, 1977.
- Newman, M.J., and R.T. Rood, Implications of solar evolution for the Earth's early atmosphere, *Science*, 198, 1035-1037, 1977.

- Nystuen, J.P., Late Precambrian Moelv Tillite deposited on a discontinuity surface associated with a fossil ice wedge, Rendalen, southern Norway, *Norsk geol. tidss.*, 56, 29-50, 1976.
- Oberbeck, V.R., J.R. Marshall, and H. Aggarwal, Impacts, tillites, and the breakup of Gondwanaland, *J. Geol.*, 101, 1-19, 1993.
- O'Connell, S., M.A. Chandler, and R. Ruedy, Implications for the creation of warm saline deep water: Late Paleocene reconstructions and global climate model simulations, *Geol. Soc. Am. Bull.*, 108, 270-284, 1996.
- Oglesby, R., and Ogg, J., The effect of large fluctuations of obliquity on climates of the Late Proterozoic, *Palaeoclimates: Data and Modeling*, 2, 293-316, 1999.
- Owen, T., R.D. Cess, and V. Ramanathan, Enhanced CO₂ greenhouse to compensate for reduced solar luminosity on early Earth, *Nature*, 277, 640-642, 1979.
- Park, J.K., Paleomagnetic constraints on the position of Laurentia from middle Neoproterozoic to Early Cambrian times, *Precamb. Res.*, 69, 95-112, 1994.
- Park, J.K., Paleomagnetic evidence for low-latitude glaciation during deposition of the Neoproterozoic Rapitan Group, Mackenzie Mountains, N.W.T., Canada, *Can. J. Earth Sci.*, 34, 34-49, 1997.
- Patrick, A., and R.C. Thunell, Tropical Pacific sea surface temperatures and upper water column thermal structure during the last glacial maximum: *Paleoceanography*, 12, 649-657, 1997.
- Peixoto, J.P., and A.H. Oort, *Physics of Climate*, Am. Inst. of Phys., New York, 520 p., 1992.
- Pelechaty, S.M., Stratigraphic evidence for the Siberia-Laurentia connection and Early Cambrian rifting, *Geology*, 24, 719-722, 1996.
- Piper, J.D.A., The Precambrian paleomagnetic record: The case for the Proterozoic supercontinent, *Earth Planet. Sci. Lett.*, 59, 61-89, 1982.
- Powell, C.McA., W.V. Preiss, C.G. Gatehouse, B. Krapez, and Z.X. Li, South Australian record of a Rodinian epicontinental basin and its mid-Neoproterozoic breakup [~700 Ma] to form the Palaeo-Pacific Ocean, *Tectonophysics*, 237, 113-140, 1994.

- Powell, C.McA., Z.X. Li, M.W. McElhinny, J.G. Meert, and J.K. Park, Paleomagnetic constraints on timing of the Neoproterozoic breakup of Rodinia and the Cambrian formation of Gondwana, *Geology*, *21*, 889-892, 1993.
- Rampino, M.R., Tillites, diamictites, and ballistic ejecta of large impacts, *J. Geol.*, *102*, 439-456, 1994.
- Rind, D., The dynamics of warm and cold climates, *J. Atmos. Sci.*, *43*, 3-24, 1986.
- Rind, D., Dependence of warm and cold climate depiction on climate model resolution, *J. Climate*, *1*, 965-997, 1988.
- Rind, D., and M.A. Chandler, Increased ocean heat transports and warmer climate, *J. Geophys. Res.*, *96*, 7437-7461, 1991.
- Rossow et al., 1982: Cloud feedback: A stabilizing effect for the early Earth? *Science*, *217*, 1245-1247.
- Rubincam, D.P., Has climate changed the Earth's tilt? *Paleoceanography*, *10*, 365-372, 1995.
- Ruddiman, W. F., and T.R. Janacek, Pliocene-Pleistocene biogenic and terrigenous fluxes at equatorial Atlantic sites 662, 663, and 664, in *Proc. ODP, Sci. Res.*, *108*, edited by W.F. Ruddiman, M. Sarnthein, J.G. Baldauf, et al., pp. 211-240, Ocean Drilling Program, College Station, Texas, 1989.
- Russell, G. L., J. R. Miller, and L. C. Tsang, Seasonal oceanic heat transports computed from an atmospheric model, *Dynam. Atmos. Oceans*, *9* 253-271, 1985.
- Sagan, C., and G. Mullen, Earth and Mars: Evolution of atmospheres and surface temperatures, *Science*, *177*, 52-56, 1972.
- Schermerhorn, L.J.G., Late Precambrian mixtites: Glacial and/or nonglacial? *Am. J. Sci.*, *274*, 673-824, 1974.
- Schmidt, P.W., and G.E. Williams, The Neoproterozoic climatic paradox: Equatorial palaeolatitude for Marinoan glaciation near sea level in South Australia, *Earth Planet. Sci. Lett.*, *134*, 107-124, 1995.

- Schmidt, P.W., G.E. Williams, and B.J.J. Emberton, Low palaeolatitude of Late Proterozoic glaciation: early timing of remanence in haematite of the Elatina Formation, South Australia, *Earth Planet. Sci. Lett.*, 105, 355-367, 1991.
- Schneider, S.H., Climate modeling, *Sci. Am.*, 256, 72-78, 1987.
- Schrag, D.P., G. Hampt, and D.W. Murray, D.W., Pore fluid constraints on the temperature and oxygen isotopic composition of the glacial ocean, *Science*, 272, 1930-1932, 1996.
- Sheldon, R.P., Ice-ring origin of the Earth's atmosphere and hydrosphere and Late Proterozoic–Cambrian phosphogenesis, *Geol. Surv. India Spec. Publ. No. 17*, 321-362, 1984.
- Sohl, L.E., *Paleoclimatology of the Neoproterozoic Interglacial to Marinoan Glacial Succession (~650-575 Ma), Central Flinders Ranges, South Australia* [Ph.D. thesis]: New York, Columbia University, 221 p., 2000.
- Sohl, L.E., Christie-Blick, N., and Kent, D.V., Paleomagnetic polarity reversals in Marinoan (ca. 600 Ma) glacial deposits of Australia: Implications for the duration of low-latitude glaciation in Neoproterozoic time: *Geological Society of America Bulletin*, 111, p. 1120-1139, 1999.
- Spencer, A.M., Late Precambrian glaciation in Scotland, *Geol. Soc. Lond. Mem.* 6, 1-48, 1971.
- Stanley, S.M., et al., *Geobiology of Critical Intervals (GOCI): A proposal for an initiative by the National Science Foundation*: Paleontological Society, 82 p., 1997.
- Thomas, G.S.P., and R.J. Connell, Iceberg drop, dump, and grounding structures from Pleistocene glacio-lacustrine sediments, Scotland, *J. Sed. Petrol.*, 55, 243-249, 1985.
- Torsvik, T.H., M.A. Smethurst, J.G. Meert, R. Van der Voo, W.S. McKerrow, M.D. Brasier, B.A. Sturt, and H.J. Walderhaug, Continental break-up and collision in the Neoproterozoic and Palaeozoic – A tale of Baltica and Laurentia, *Earth-Sci. Rev.*, 40, 229-258, 1996.
- Torsvik, T.H., M.A. Smethurst, R. Van der Voo, A. Trench, N. Abrahamsen, N., and E. Halvorsen, E., Baltica. A synopsis of Vendian-Permian palaeomagnetic data and their palaeotectonic implications, *Earth-Sci. Rev.*, 33, 133-152, 1992.

- Trenberth, K.E., and A. Solomon, The global heat balance: Heat transports in the atmosphere and ocean, *Clim. Dynam.*, *10*, 107-134, 1994.
- Van der Voo, R., The reliability of paleomagnetic data: *Tectonophysics*, *184*, 1-9, 1990.
- Van der Voo., R., J.C. Briden, and B.A. Duff, Late Precambrian and Paleozoic paleomagnetism of the Atlantic bordering continents, in *Geology of Europe, From Precambrian to the Post-Hercynian Sedimentary Basins*, coordinated by J. Cogne and M. Slansky, Bur. Recherch. Geol. Min. (BRGM), n. 108, pp. 203-212, 1980.
- Veevers, J.J., M.R. Walter, and E. Scheibner, Neoproterozoic tectonics of Australia-Antarctica and Laurentia and the 560 Ma birth of the Pacific Ocean reflect the 400 m.y. Pangean supercycle, *J. Geol.*, *105*, 225-242, 1997.
- Vorren, T.O., M. Hald, M. Edvardsen, and O.D. Lind-Hansen, Glacigenic sediments and sedimentary environments on continental shelves: General principles with a case study from the Norwegian shelf, in *Glacial Deposits in North-West Europe*, edited by J. Ehlers, pp. 61-73, A.A. Balkema, Rotterdam, 1983.
- Ward, W.R., Comments on the long-term stability of the Earth's obliquity, *Icarus*, *50*, 444-448, 1982.
- Walter, M.R., and J. Bauld, The association of sulphate evaporites, stromatolitic carbonates and glacial sediments; examples from the Proterozoic of Australia and the Cenozoic of Antarctica, *Precambr. Res.*, *21*, 129-148, 1983.
- Webb, R.S., D.H. Rind, S.J. Lehman, R.J. Healy, and D. Sigman, Influence of ocean heat transport on the climate of the Last Glacial Maximum, *Nature*, *385*, 695-699, 1997.
- Williams, D.M., J.F. Kasting, and L.A. Frakes, Low-latitude glaciation and rapid changes in the Earth's obliquity explained by obliquity-oblateness feedback, *Nature*, *396*, 453-455, 1998.
- Williams, G.E., Late Precambrian glacial climate and the Earth's obliquity, *Geol. Mag.*, *112*, 441-465, 1975.
- Williams, G.E., History of the Earth's obliquity, *Earth-Sci. Rev.*, *34*, 1-45, 1993.

- Williams, G.E., The enigmatic late Proterozoic glacial climate: An Australian perspective, in *Earth's Glacial Record*, edited by M. Deynoux, J.M.G. Miller, E.W. Domack, N. Eyles, I.J. Fairchild, and G.M. Young, pp. 146-164, Cambridge Univ. Press, Cambridge, United Kingdom, 1994a.
- Williams, G.E., Resonances of the fluid core for a tidally decelerating Earth: Cause of increased plume activity and tectonothermal reworking events? *Earth Planet. Sci. Lett.*, 128, 155-167, 1994b.
- Williams, G.E., and D.G. Tonkin, Periglacial structures and palaeoclimatic significance of a late Precambrian block field in the Cattle Grid copper mine, Mount Gunson, South Australia, *Austral. J. Earth Sci.*, 32, 287-300, 1985.
- Worsley, T.R., and D.L. Kidder, First-order coupling of paleogeography and CO₂, with global surface temperature and its latitudinal contrast, *Geology*, 19, 1161-1164, 1991.
- Zhang, H. and W. Zhang, Paleomagnetic data, late Precambrian magnetostratigraphy and tectonic evolution of eastern China, *Precambr. Res.*, 29, 65-75, 1985.
- Zhang Qi Rui, Environmental evolution during the early phase of Late Proterozoic glaciation, Hunan, China, in *Earth's Glacial Record*, edited by M. Deynoux, J.M.G. Miller, E.W. Domack, N. Eyles, I.J. Fairchild, and G.M. Young, pp. 260-266, Cambridge Univ. Press, Cambridge, United Kingdom, 1994.
- Zhang, Y.-C., and W. Rossow, Estimating meridional energy transports by the atmospheric and oceanic general circulations using boundary flux data, *J. Climate* 10, 2358-2373, 1997.

FIGURE CAPTIONS

Fig. 1. Earth history context for the Varanger glacial interval. The close temporal relationship between the end of the Varanger glacial interval and the rise of metazoans is of great interest to the paleobiology community; there has been a great deal of discussion about the extent to which dramatic climatic changes may have spurred evolutionary development of complex multicellular life (e.g., *Knoll [1992a]*, *Stanley et al. [1997]*). Proposed formal stratigraphic subdivisions of the Neoproterozoic Era follow *Cowie et al. [1989]*. Boundaries between informal climatic subdivisions [*Sohl, 2000*] are dashed to reflect the uncertainty in dating the transition from one climatic mode to another. Ages given for geologic events are approximate, owing to sparse radiometric constraints in most cases. Tectonic events: *Moores [1991]*, *Hoffman [1991]*, *Powell et al. [1993]*, *Meert and van der Voo [1997]*, *Dalziel [1997]*. Biological events: see summary in *Conway Morris [1993]*; see also *Hofmann et al. [1990]*, *Knoll [1992b]*, *Bromham et al. [1998]*. *Grotzinger et al. [1995]*. Environmental events: *Knoll and Walter [1992]*, *Schmidt and Williams [1995]*, *Canfield and Teske [1996]*, *Park [1997]*, *Sohl et al. [1999]*.

FIG. 2. Mollweide map projection of continental distribution during the Varanger glacial interval, ~600 Ma, as used in this study. 1 = North China; 2 = Tibet; 3 = Australia; 4 = India; 5 = East Antarctica; 6 = Kalahari Craton; 7 = Congo Craton; 8 = South China; 9 = North America (Laurentia); 10 = Greenland; 11 = Baltica; 12 = Siberia; 13 = Kazakhstan; 14 = Mongolia; 15 = Armorica; 16 = Amazonia/São Francisco/La Plata; 17 = West Africa. The locations of glacial deposits are marked by stars or by a “?” if their origin is uncertain.

FIG. 3. Zonally averaged meridional ocean heat transports for three Varanger scenarios and for the GISS GCM current climate control run.

FIG. 4. Annual mean, global surface air temperature in the GCM through the 60 years of simulation. All simulations ran for reached equilibrium except the obliquity simulation which ran for only 6 years.

FIG. 5. Surface Air Temperatures. Individual maps are labelled according to the forcings applied in the simulations. All simulations except Modern used the Varanger paleogeographic reconstruction.

FIG. 6.–Snow and Ice Coverage [see legend Figure 5].

FIG. 7. Zonal mean, annual average anomalies of: (a) surface air temperature, (b) water vapor and (c) total cloud cover, for the two altered ocean heat transport scenarios. The change is the difference between the ocean heat transport simulations and the Varanger paleogeographic control run, which used modern ocean heat transports.

FIG. 8.–Global surface air temperature plotted vs. continental snow cover, ocean ice cover, and snow depth over land. Values are mean annual results. Both snow and ocean ice coverage are negatively correlated with surface air temperature, whereas snow depth peaks at about 10°C and declines in both warmer and colder Varanger climate scenarios. Snow depth tends to decrease as ice cover increases, but at very low ice cover values [i.e., very warm climates], snow on land rapidly disappears.

Table 1. List of simulations and climate forcings. Simulation labels corresponds to those used in other tables and on the color maps in figures 5 and 6.

Simulation Label	Continental Distribution	Solar Luminosity (1.0 = modern)	Atmospheric CO ₂ (ppm)	Ocean Heat Transport (1.0 = modern)	Obliquity
M.	Modern	1.0	315	1.0	23.5°
V.	Varanger	1.0	315	1.0	23.5°
1.	Varanger	1.0	1260	1.0	23.5°
2.	Varanger	1.0	1260	0.5	23.5°
3.	Varanger	1.0	315	0.5	23.5°
4.	Varanger	0.94	1260	0.5	23.5°
5.	Varanger	1.0	140	1.0	23.5°
6.	Varanger	1.0	315	1.5	23.5°
7.	Varanger	0.94	315	1.0	23.5°
8.	Varanger	1.0	40	1.0	23.5°
9.	Varanger	1.0	315	1.0	60.0°
10.	Varanger	0.94	315	0.5	23.5°
11.	Varanger	0.94	140	1.0	23.5°
12.	Varanger	0.94	140	0.5	23.5°
13.	Varanger	0.94	40	0.5	23.5°

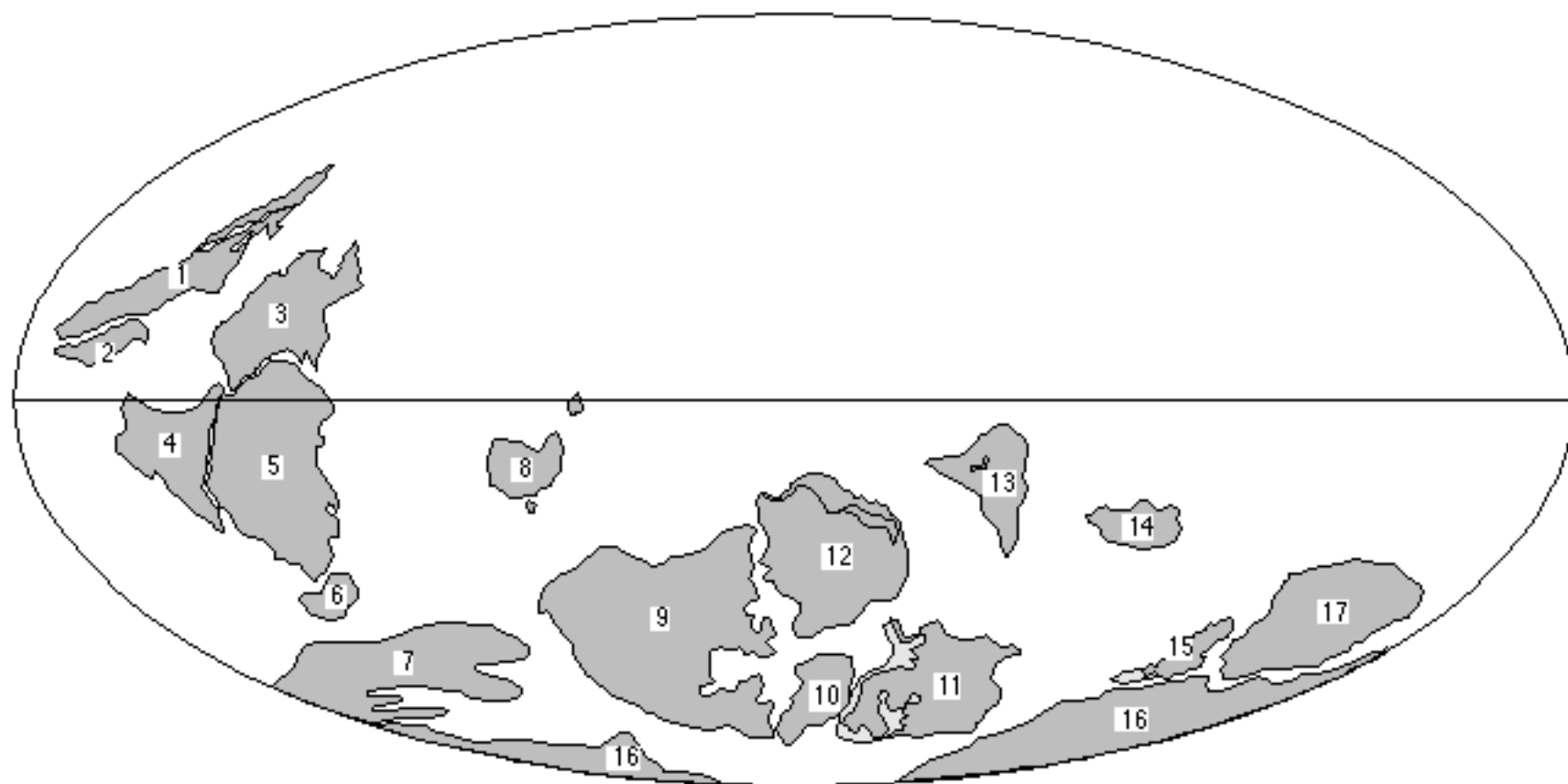
Table 2.Values for surface air temprature, continental snow coverage, and key climate feedback quantities. Forcings that were altered for each simulation are shown, other forcings are the same as in the modern climate control run (M). All Varanger simulations (V) use the paleocontinental reconstruction (see figure 2) as a land surface boundary condition.

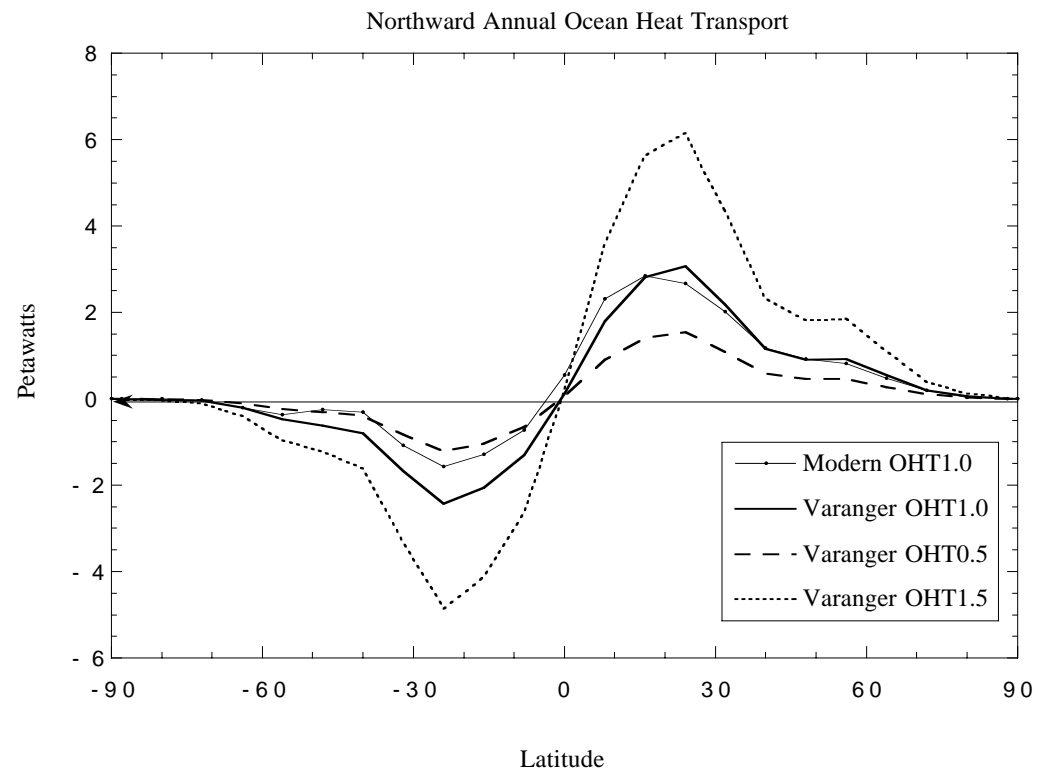
Simulation	Altered Forcings	Surface Air Temperature		Snow Over Land		Cloud Cover Amount		Albedo		Atm. Water Vapor
		Tropical (°C at 4°N)	Global Mean (°C)	Cover (%)	Depth (m)	Low Level {%}	High Level (%)	Planetary (%)	Surface (%)	(mm H ₂ O)
M (Modern)	Sol. Lum.=1.0 CO ₂ =315 ppm OHT=1.0 Obliq.=23.5°	25.1	13.4	24.2	0.2	36.7	28.4	30.3	12.0	23.7
V (Varanger)	continental distribution	25.4	14.3	35.1	26.5	36.2	29.6	28.5	9.54	24.7
V1	CO ₂ =1260 ppm	36.6	28.1	10.7	0.08	24.1	15.3	21.7	6.64	59.9
V2	CO ₂ =1260 ppm OHT=0.5	36.1	24.6	16.8	0.15	28.9	16.9	23.9	6.86	49.9
V3	OHT=0.5	22.9	7.6	44.2	25.4	41.7	28.9	32.5	14.4	17.4
V4	CO ₂ =1260 ppm Sol. Lum.=0.94	22.2	11.7	38.2	25.7	35.9	29.4	28.8	10.6	19.5
V5	CO ₂ =140 ppm	19.9	6.9	46.6	27.4	39.8	27.4	31.6	14.2	15.4
V6	OHT=1.5	16.8	11.4	36.5	21.2	39.4	27.9	30.2	10.1	18.7

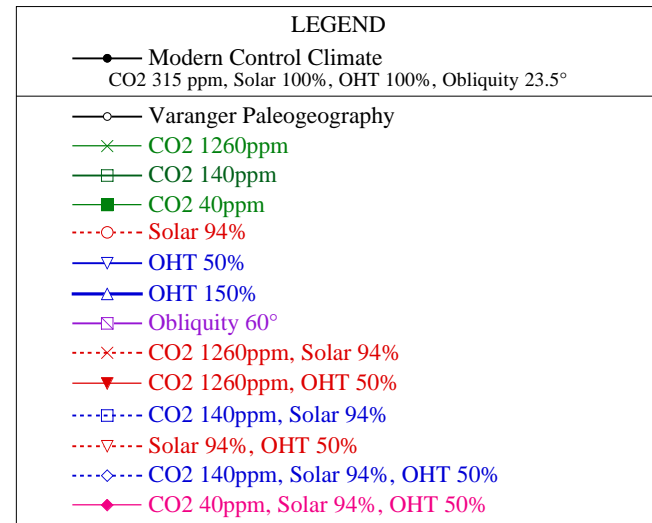
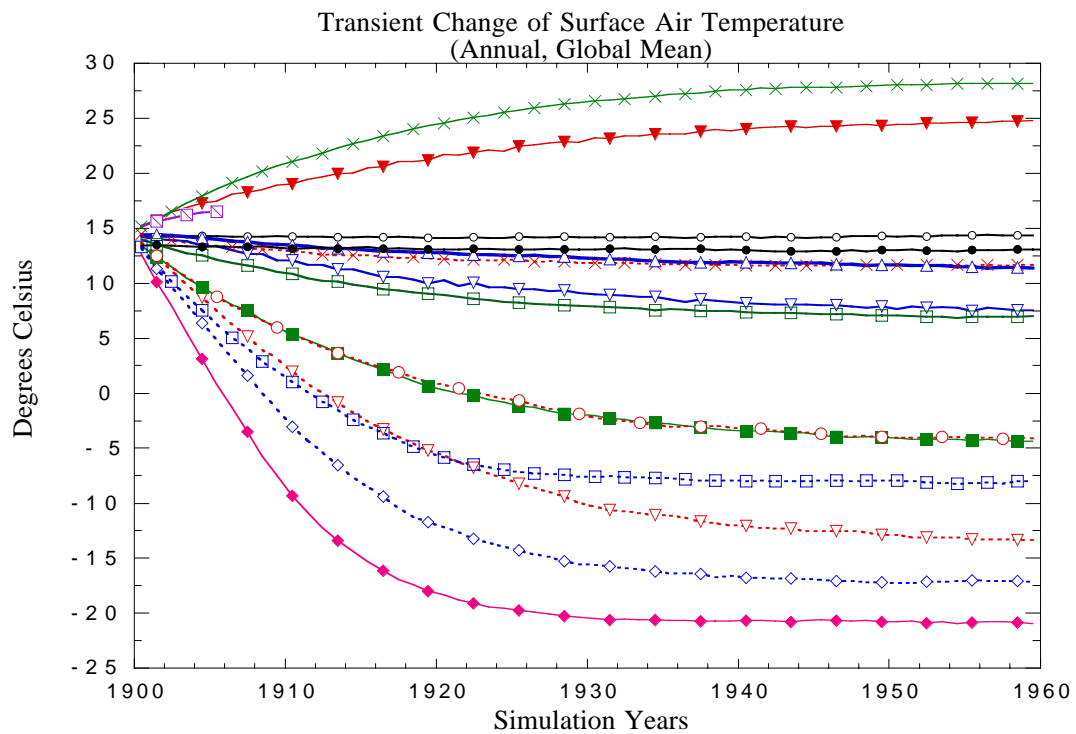
Table 2. Continued...

V7	Sol. Lum.=0.94	9.4	-4.0	71.0	21.0	43.9	26.4	36.3	23.5	7.1
V8	CO ₂ =40 ppm	8.9	-4.3	69.4	21.4	46.8	25.6	37.3	23.7	7.3
V9	Obliq.=60°	7.5	16.4	8.9	0.04	31.8	28.5	26.9	7.95	25.5
V10	Sol. Lum.=0.94 OHT=0.5	7.0	-13.3	75.6	17.9	47.1	24.4	41.4	34.7	4.18
V11	CO ₂ =140 ppm Sol. Lum.=0.94	6.4	-8.1	90.5	20.2	45.1	24.7	37.8	27.1	5.4
V12	CO ₂ =140 ppm Sol. Lum.=0.94 OHT=0.5	4.0	-17.1	84.0	15.1	47.4	22.6	42.8	37.8	3.1
V13	CO ₂ =40 ppm Sol. Lum.=0.94 OHT=0.5	-1.1	-20.8	100.	11.9	47.5	20.3	44.0	40.3	2.2

Age (Ma)	Geologic Time	Informal Climatic Subdivisions	Geologic Events		
			Tectonic	Biological	Environmental
550	Phanerozoic Era Neoproterozoic Era Tonian	Post-Varanger Warm Interval	Gondwana assembly complete Brasiliano Orogeny Pannotia supercontinent? East African Orogeny Pan-African orogenic events Rodinia breakup Assembly of Rodinian supercontinent complete	"Cambrian explosion"	Ediacaran fauna abundant; first small shelly fossils First appearance of primitive Ediacaran-type fauna Multicellular algae abundant Early divergence of metazoan phyla? Widespread glaciation; low-latitude glacial event confirmed Widespread glaciation; low-latitude glacial event probable Oxygenation event brings atmospheric O ₂ to 0.1 PAL
600		Varanger Glacial Interval			
650		Interglacial			
700		Sturtian Glacial Interval			
750					
800					
850		Pre-Sturtian Warm Interval			
900					
950					
1000					
	Mesoproterozoic Era				







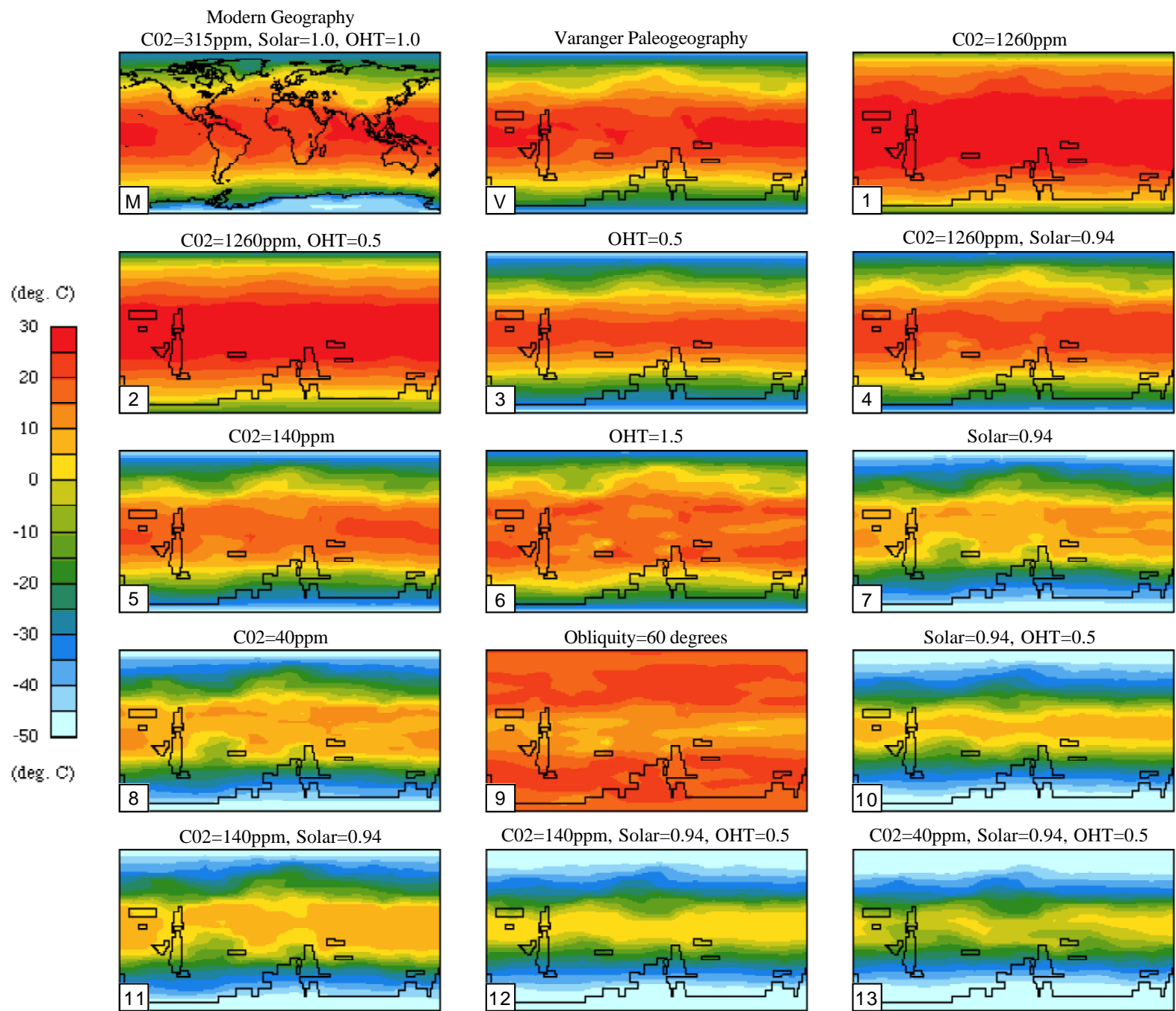


Figure 5. Surface Air Temperature

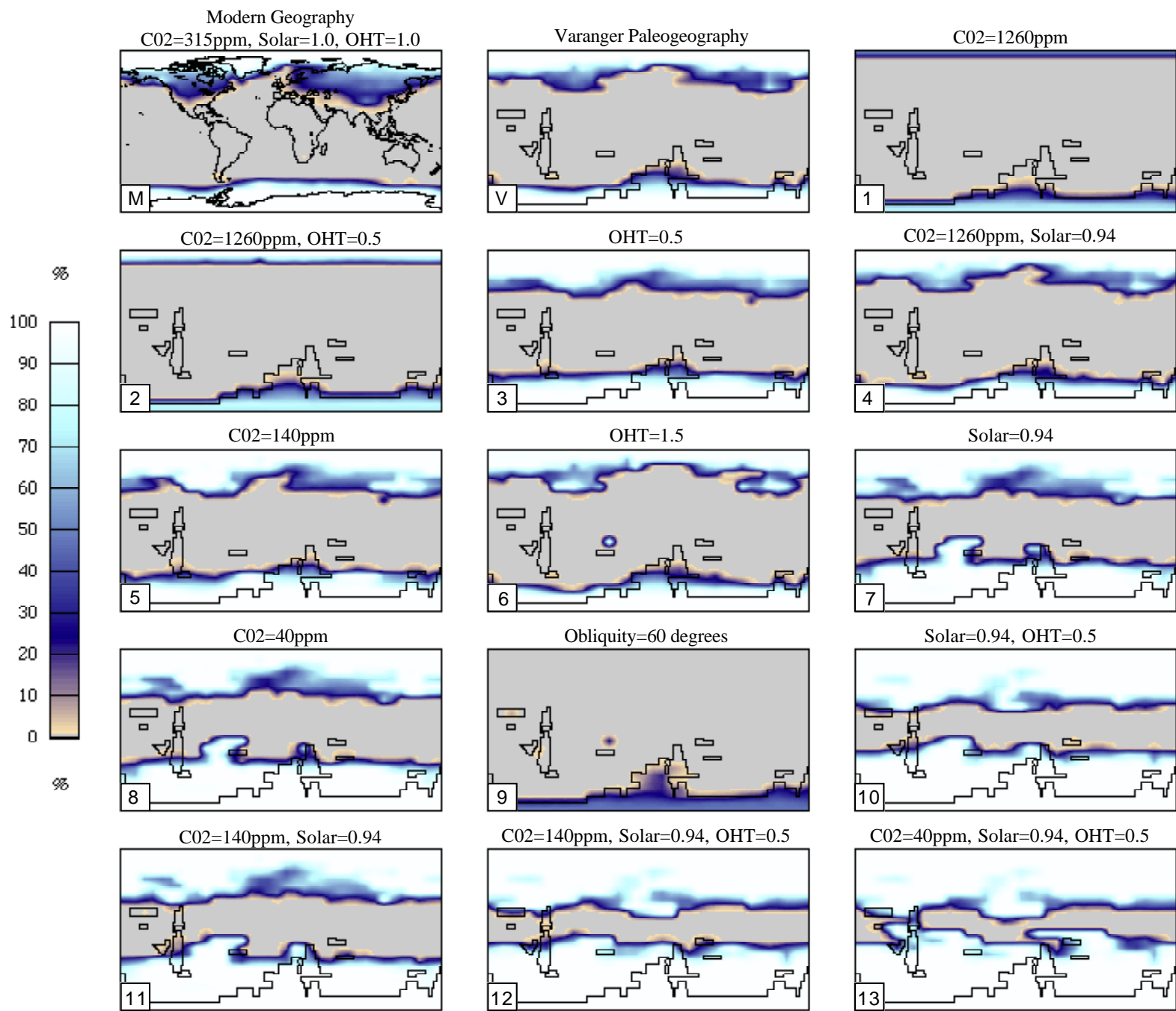
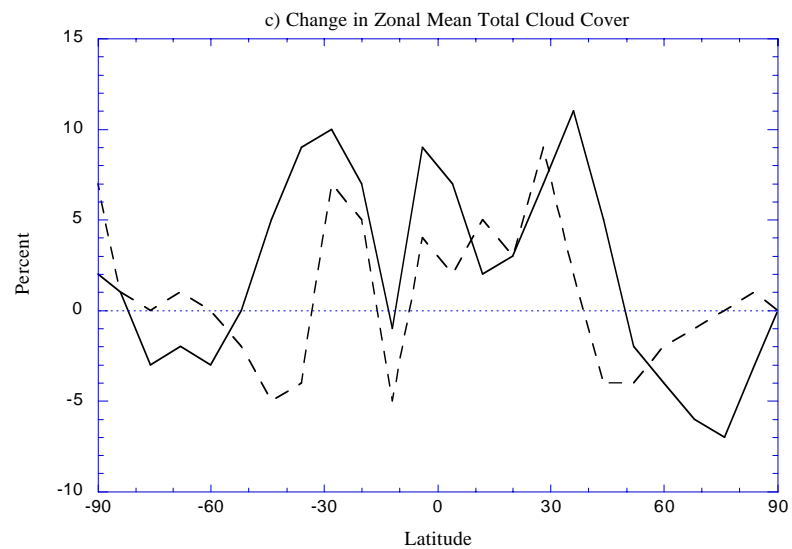
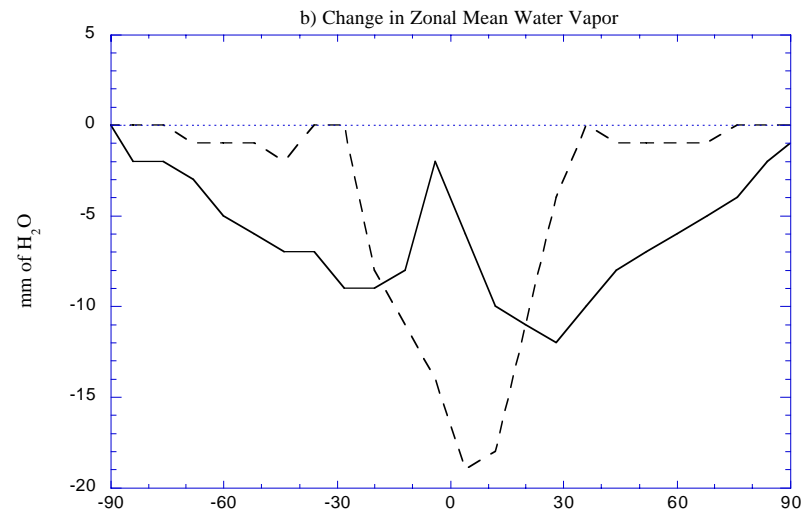
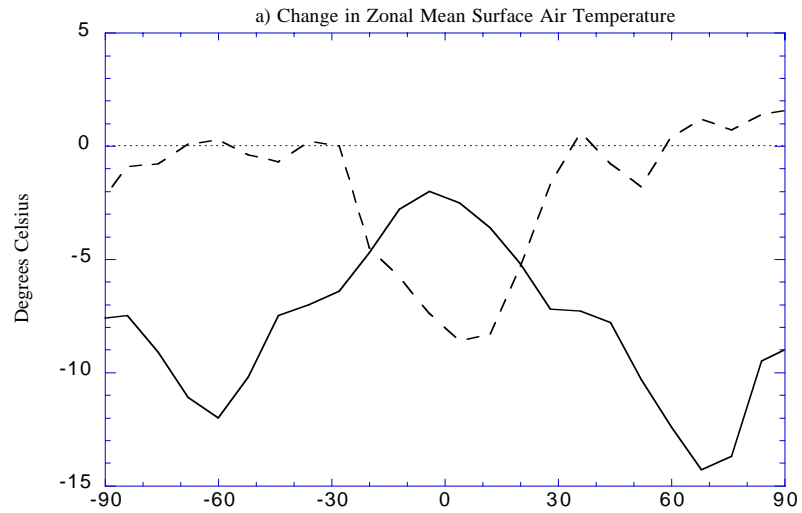


Figure 6. Snow and Ice Cover



-- -OHT1.5 - OHT1.0

— OHT0.5 - OHT1.0

